American Mineralogist, Volume 97, pages 1402–1416, 2012

Limitations of Fe^{2+} and Mn^{2+} site occupancy in tourmaline: Evidence from Fe^{2+}- and Mn^{2+}-rich tourmaline†

Andreas Ertl,[1,*] Uwe Kolitsch,[2,1] M. Darby Dyar,[3] John M. Hughes,[4] George R. Rossman,[5] Adam Pieczka,[6] Darrell J. Henry,[7] Federico Pezzotta,[8] Stefan Prowatke,[9] Christian L. Lengauer,[1] Wilfried Körner,[10] Franz Brandstätter,[2] Carl A. Francis,[11] Markus Prem,[1] and Ekkehart Tillmanns[1]

[1]Institut für Mineralogie und Kristallographie, Geozentrum, Universität Wien, Althanstrasse 14, 1090 Vienna, Austria
[2]Mineralogisch-Petrographische Abt., Naturhistorisches Museum, Burgring 7, 1010 Vienna, Austria
[3]Department of Geography and Geology, Mount Holyoke College, South Hadley, Massachusetts 01075, U.S.A.
[4]Department of Geology, University of Vermont, Delehanty Hall, Burlington, Vermont 05405, U.S.A.
[5]Division of Geological and Planetary Sciences, California Institute of Technology, Pasadena 91125-2500, U.S.A.
[6]Department of Mineralogy, Petrography, and Geochemistry, AGH University of Science and Technology, al. Mickiewicza 30, 30-059 Kraków, Poland
[7]Department of Geology and Geophysics, Louisiana State University, Baton Rouge, Louisiana 70803, U.S.A.
[8]Museo di Storia Naturale, Corso Venezia 55, I-20121 Milan, Italy
[9]Institut für Geowissenschaften, Universität Heidelberg, Im Neuenheimer Feld 236, 69120 Heidelberg, Germany
[10]Department für Umweltgeowissenschaften, Geozentrum, Universität Wien, Althanstrasse 14, 1090 Vienna, Austria
[11]Harvard Mineralogical Museum, 24 Oxford Street, Cambridge, Massachusetts 02138, U.S.A.

Abstract

Fe^{2+}- and Mn^{2+}-rich tourmalines were used to test whether Fe^{2+} and Mn^{2+} substitute on the *Z* site of tourmaline to a detectable degree. Fe-rich tourmaline from a pegmatite from Lower Austria was characterized by crystal-structure refinement, chemical analyses, and Mössbauer and optical spectroscopy. The sample has large amounts of Fe^{2+} (~2.3 apfu), and substantial amounts of Fe^{3+} (~1.0 apfu). On basis of the collected data, the structural refinement and the spectroscopic data, an initial formula was determined by assigning the entire amount of Fe^{3+} (no delocalized electrons) and Ti^{4+} to the *Z* site and the amount of Fe^{2+} and Fe^{3+} from delocalized electrons to the *Y*-*Z* ED doublet (delocalized electrons between *Y*-*Z* and *Y*-*Y*): $^{X}(Na_{0.9}Ca_{0.1})\ ^{Y}(Fe^{2+}_{2.0}Al_{0.4}Mn^{2+}_{0.3}Fe^{3+}_{0.2})\ ^{Z}(Al_{4.8}Fe^{3+}_{0.8}Fe^{2+}_{0.2}Ti^{4+}_{0.1})\ ^{T}(Si_{5.9}Al_{0.1})O_{18}\ (BO_3)_3\ ^{V}(OH)_3\ ^{W}[O_{0.5}F_{0.3}(OH)_{0.2}]$ with $a = 16.039(1)$ and $c = 7.254(1)$ Å. This formula is consistent with lack of Fe^{2+} at the *Z* site, apart from that occupancy connected with delocalization of a hopping electron.

The formula was further modified by considering two ED doublets to yield: $^{X}(Na_{0.9}Ca_{0.1})\ ^{Y}(Fe^{2+}_{1.8}Al_{0.5}Mn^{2+}_{0.3}Fe^{3+}_{0.3})\ ^{Z}(Al_{4.8}Fe^{3+}_{0.7}Fe^{2+}_{0.4}Ti^{4+}_{0.1})\ ^{T}(Si_{5.9}Al_{0.1})O_{18}\ (BO_3)_3\ ^{V}(OH)_3\ ^{W}[O_{0.5}F_{0.3}(OH)_{0.2}]$. This formula requires some Fe^{2+} (~0.3 apfu) at the *Z* site, apart from that connected with delocalization of a hopping electron. Optical spectra were recorded from this sample as well as from two other Fe^{2+}-rich tourmalines to determine if there is any evidence for Fe^{2+} at *Y* and *Z* sites. If Fe^{2+} were to occupy two different 6-coordinated sites in significant amounts and if these polyhedra have different geometries or metal-oxygen distances, bands from each site should be observed. However, even in high-quality spectra we see no evidence for such a doubling of the bands. We conclude that there is no ultimate proof for Fe^{2+} at the *Z* site, apart from that occupancy connected with delocalization of hopping electrons involving Fe cations at the *Y* and *Z* sites.

A very Mn-rich tourmaline from a pegmatite on Elba Island, Italy, was characterized by crystal-structure determination, chemical analyses, and optical spectroscopy. The optimized structural formula is $^{X}(Na_{0.6}\square_{0.4})\ ^{Y}(Mn^{2+}_{1.3}Al_{1.2}Li_{0.5})\ ^{Z}Al_6\ ^{T}Si_6O_{18}\ (BO_3)_3\ ^{V}(OH)_3\ ^{W}[F_{0.5}O_{0.5}]$, with $a = 15.951(2)$ and $c = 7.138(1)$ Å. Within a 3σ error there is no evidence for Mn occupancy at the *Z* site by refinement of Al ↔ Mn, and, thus, no final proof for Mn^{2+} at the *Z* site, either.

Oxidation of these tourmalines at 700–750 °C and 1 bar for 10–72 h converted Fe^{2+} to Fe^{3+} and Mn^{2+} to Mn^{3+} with concomitant exchange with Al of the *Z* site. The refined ^{Z}Fe content in the Fe-rich tourmaline increased by ~40% relative to its initial occupancy. The refined ^{Y}Fe content was smaller and the <*Y*-O> distance was significantly reduced relative to the unoxidized sample. A similar effect was observed for the oxidized Mn^{2+}-rich tourmaline. Simultaneously, H and F were expelled from both samples as indicated by structural refinements, and H expulsion was indicated by infrared spectroscopy. The final species after oxidizing the Fe^{2+}-rich tourmaline is buergerite. Its color had changed from blackish to brown-red. After oxidizing the Mn^{2+}-rich tourmaline, the previously dark yellow sample was very dark brown-red, as expected for the oxidation of Mn^{2+} to Mn^{3+}. The unit-cell parameter *a* decreased during oxidation whereas the *c* parameter showed a slight increase.

Keywords: Mn^{2+}-rich tourmaline, Fe^{2+}-rich tourmaline, Mössbauer, crystal structure, lower Austria, Elba Island, Italy, site occupancy

* E-mail: andreas.ertl@a1.net
† Open Access, thanks to the author's funding. Article available to all readers via GSW (http://ammin.geoscienceworld.org) and the MSA web site.

INTRODUCTION

The general chemical formula of tourmaline-supergroup minerals can be written as $X\,Y_3\,Z_6\,[T_6O_{18}]\,(BO_3)_3\,V_3\,W$, as proposed by Henry et al. (2011). These authors and Hawthorne (1996, 2002) suggest occupancies at these sites as follows:

X = Ca, Na, K, □ (vacancy);
Y = Li, Mg, Fe^{2+}, Mn^{2+}, Al, Cr^{3+}, V^{3+}, Fe^{3+};
Z = Mg, Al, Fe^{3+}, V^{3+}, Cr^{3+};
T = Si, Al, B;
V = OH, O;
W = OH, F, O.

One of the issues concerning the proposed site occupancies is whether Fe^{2+} or Mn^{2+} can occupy the Z site to a significant degree. Structural and chemical studies of Fe^{2+}-rich tourmalines by Grice and Ercit (1993), Bloodaxe et al. (1999), Francis et al. (1999), and Cámara et al. (2002) found no evidence for significant amounts of Fe^{2+} on the Z site, consistent with the site assignments of Hawthorne and Henry (1999). Furthermore, based on the changes in mean sizes of the Y- and Z-centered octahedra of thermally oxidized Fe-rich tourmalines, Pieczka and Kraczka (2001, 2004) and Kraczka and Pieczka (2000) concluded that Fe^{2+} (and Mn^{2+}) occupies only the Y octahedral sites. Similarly, Mn^{2+}-rich tourmalines, structurally and chemically characterized by Nuber and Schmetzer (1981), Burns et al. (1994), and Ertl et al. (2003, 2004b), did not exhibit any evidence of Mn^{2+} at the Z site. In contrast, Bosi and Lucchesi (2004), Bosi et al. (2005a, 2005b), and Bosi (2008) interpreted their structural and chemical studies on tourmaline as having up to ~0.26 atoms per formula unit (apfu) Fe^{2+} and up to ~0.10 apfu Mn^{2+} in the Z site. Their Mössbauer studies indicated that all Fe is in octahedral coordination (Bosi and Lucchesi 2004). In addition, Bosi and Lucchesi (2007) reinterpreted Fe^{2+} occupancy in previously determined tourmaline structures and suggested Fe^{2+} occupancies in the Z site of as much as 0.70 apfu. In their Mössbauer study, Andreozzi et al. (2008) described a doublet, which they consider consistent with Fe^{2+} in the Z octahedron. Also in this paper, they reported new Mössbauer spectra from the same samples used by Bosi and Lucchesi (2004) and Bosi et al. (2005b). Using the chemical composition from the Bosi papers, they determined site assignments from their newly obtained spectra that corroborate the occupation of Fe^{2+} at the Z site of the original papers. The average deviation, compared with the site assignments from the original publications (by using chemistry, structural data and an optimization program), is only 0.01 apfu Fe^{2+}. Recently, Bačik et al. (2011a) reported only negligible contents of Fe^{2+} at the Z site of Fe^{2+}-rich tourmalines.

To resolve the apparent disagreement over the presence of significant Fe^{2+} and Mn^{2+} on the Z site in tourmaline, we have investigated two samples—one that is unusually rich in Fe^{2+} and the other rich in Mn^{2+}. The Fe^{2+}-rich and Mn^{2+}-rich tourmaline samples were characterized with a combination of crystal-structure determinations, electron microprobe analysis (EMPA), inductively coupled plasma-mass spectroscopy (ICP-MS) analysis, Mössbauer, and optical spectroscopy. In turn, these tourmalines were heat-treated under oxidizing conditions to investigate the consequences of conversion of divalent cations to trivalent cations on the site occupancies. For comparison, another two Fe^{2+}-rich tourmaline samples described originally by Cámara et al. (2002) and Ertl et al. (2006b) were investigated by optical spectroscopy.

PETROLOGICAL SETTINGS OF SAMPLES

The tourmaline samples are from petrologic environments that are consistent with the crystallization of Fe-rich and Mn-rich tourmaline. An unusually Fe-rich tourmaline sample (BLS1/BLS2) was collected from a metamorphosed pegmatite from Blocherleitengraben, Lower Austria (Ertl 1995) (WGS84 N 48°23′42″/E 015°24′05″). It is associated with magnetite, pyrite, spessartine, biotite, albite, microcline, and quartz. This Variscan pegmatite, which is situated in the Mühldorf nappe embedded in paragneisses and calc-silicate rock of the Drosendorf unit ("Varied Series"), belongs to the Moldanubic nappes, which form large parts of the Bohemian massif in Lower Austria (Fuchs and Matura 1976).

The Mn^{2+}-rich tourmaline sample (MNELB3) is from a Li-Cs-Ta-enriched (LCT) pegmatite mined in 1994–1995 in the Fosso dei Forcioni, near San Ilario (Sant'Ilario) in Campo, on Elba, Italy (Orlandi and Pezzotta 1996; Aurisicchio and Pezzotta 1997). This pegmatite, up to 30 cm across and about 7 m in length, dips 70° to the west and is hosted in the Oligocene monzogranite of the Mount Capanne pluton. The center of the vein (now mined out) was characterized by a series of miarolitic cavities lined by drusy crystals of feldspars, quartz, and polychrome tourmalines (elbaite-rossmanite-schorl series) up to 2.5 cm in length. Accessory minerals, which are rare constituents of the cavities, include beryl, lepidolite, cassiterite, U-rich microlite, and very rare pollucite. It is important to note that garnet (spessartine) is totally lacking in this vein and, in Elba pegmatites, this lack of garnet corresponds to a strong enrichment of Mn^{2+} in tourmaline crystals.

EXPERIMENTAL DETAILS

Crystal-structure refinement

The tourmaline X-ray diffraction data were collected at ambient temperature with either a Bruker Apex CCD or a Nonius Kappa CCD single-crystal diffractometer using graphite-monochromatized Mo$K\alpha$ radiation. Crystal data, data collection information, and refinement details are given in Table 1. Redundant data were collected for an approximate sphere of reciprocal space, and were integrated and corrected for Lorentz and polarization factors, and absorption correction, using the Bruker programs SaintPlus and SADABS for BLS1 (Bruker AXS Inc. 2001) or the Nonius programs COLLECT and DENZO-SMN (Nonius 2007) and multi-scan absorption correction (Otwinowski et al. 2003) for the remaining samples. The structures were refined with SHELXL-97 (Sheldrick 2008), except BLS1 (SHELXTL 6.12; Bruker AXS Inc. 2001), using scattering factors for neutral atoms. During all refinements, the X site was modeled with Na scattering factors and unconstrained multiplicity, and the Y site and Z site were similarly modeled using Al and Fe scattering factors in Fe-rich tourmaline as well as Al and Mn in Mn-rich tourmaline. The T site was modeled using Si scattering factors, but with fixed occupancy of $Si_{1.00}$, because refinement with unconstrained multiplicity showed this site to be essentially fully occupied by Si within error limits. The B site was modeled with fixed occupancy of $B_{1.00}$. The H site was freely refined. Refinement was performed with anisotropic thermal parameters for all non-hydrogen atoms. Table 2 lists the atom parameters, and Table 3 presents selected interatomic distances.

Chemical analyses

The Fe^{2+}-rich sample (BLS1, from Blocherleitengraben, Lower Austria) used for chemical analysis and structural formula calculation was a small fragment

extracted from the core of a black tourmaline crystal (~1 cm in diameter). Sample BLS2 (small fragment extracted from an area near the core of the same tourmaline crystal), which has a refined structural formula very similar to that of BLS1 (see below), was not chemically analyzed. The Mn^{2+}-rich sample (MNELB3 from Elba, Italy) was a dark yellow fragment taken from the most Mn^{2+}-rich zone of a yellowish tourmaline crystal that was ~7 mm long and ~5 mm in diameter. Electron microprobe analyses were obtained with a Cameca SX51 electron microprobe equipped with five wavelength-dispersive spectrometers. Operating conditions were 15 kV accelerating voltage, 20 nA beam current, and a 5 µm beam diameter. Peaks for all elements were measured for 10 s, except for Mg (20 s), Cr (20 s), Ti (20 s), Zn (30 s), and F (40 s). Because the F*K*α line interferes with the Fe*L*α and Mn*L*α lines, the measured F values require a correction. Ertl et al. (2009) give the following formula for correcting this interference: $F = F_{meas} - (-0.000055\ FeO^2 + 0.00889\ FeO - 0.0044) + 0.015\ MnO$. Natural and synthetic silicates and oxides were used as standards (Ertl et al. 2003). The analytical data were reduced and corrected using the PAP routine (Pouchou and Pichoir 1991). A modified matrix correction was applied assuming stoichiometric O atoms and all non-measured components as B_2O_3. The latter was calculated assuming B = 3.00 apfu and because there was no clear evidence for $^{[4]}$B in either investigated tourmaline sample (<*T*-O> distance is in the range 1.622–1.623 Å; Table 3). The accuracy of the electron-microprobe analyses and the correction procedure was checked by analyzing three reference tourmalines (98114: elbaite, 108796: dravite, 112566: schorl). Compositions of these tourmaline samples are presented in the context of an interlaboratory comparison study (Dyar et al. 1998, 2001). Under the described conditions, analytical errors on all analyses are ±1% relative to major elements and ±5% relative to minor elements (Table 4).

The sample preparation for ICP-MS analysis was performed in a clean laboratory using ultrapure acids. To remove surface contamination, the tourmaline grains were leached in 2.5 *N* HCl for 15 min at about 80 °C. Sample digestion was performed in tightly sealed polytetrafluoroethylene beakers using a 3:1 HF/HNO_3 mixture. After about 2 weeks at ~150 °C, the samples were evaporated and transformed into nitrates using HNO_3. ICP-MS analyses were performed on an ELAN 6100 (Perkin Elmer/SCIEX; University of Vienna).

To determine the OH content of the tourmaline samples, ~32 mg of the core material of the Fe-rich tourmaline crystal and ~20 mg of the Mn-rich elbaite were used for thermogravimetric analysis (TGA), performed on a Mettler-Toledo TGA/SDTA 851 (University of Vienna). The powder was heated from 25 to 1100 °C (5 °C/min) in N_2 gas (gas flow: 25 mL/min). To determine the stability under the (O_2-bearing) atmosphere we heated ~32 mg powder of the schorl sample up to 1100 °C under air.

Mössbauer analysis

Approximately 10 mg of each $Fe^{2+/3+}$-rich sample (natural and oxidized) was gently crushed under acetone, then mixed with a sugar-acetone solution designed to form sugar coatings around each grain and prevent preferred orientation. Grains were heaped in a sample holder confined by Kapton tape. Mössbauer spectra were acquired at 295 K using a source of 40 mCi ^{57}Co in Rh on a WEB Research Co. model WT302 spectrometer (Mount Holyoke College) and corrected to remove the fraction of the baseline due to the Compton scattering of 122 keV γ rays by electrons inside the detector. Run times were 24 h with baseline counts of 9 and 32 million. Spectra were collected in 2048 channels and corrected for nonlinearity. Data were modeled using a program from the University of Ghent, in Belgium called DIST_3E (an implementation of software described in Wivel and Mørup 1981), which uses model-independent quadrupole splitting distributions for which the subspectra are constituted by Lorentzian-shaped lines. Peak areas were not corrected for differential recoil-free fractions for Fe^{2+} and Fe^{3+} because the appropriate correction factors do not exist.

Optical spectra

Approximately 5 × 10 mm crystal fragments of both the unheated and heated $Fe^{2+/3+}$-rich tourmaline were prepared as doubly polished 0.030 mm thick thin-sections. Approximately 3 × 8 mm crystal fragments of both the unheated and heated $Mn^{2+/3+}$-rich tourmaline were prepared as ~0.6 mm thick doubly polished plates. Polarized optical absorption spectra in the 390–1100 nm range were obtained at about one nm resolution with a locally built microspectrometer system (California Institute of Technology, Pasadena) consisting of a 1024-element Si diode-array detector coupled to a grating spectrometer system via fiber optics to a highly modified NicPlan infrared microscope containing a calcite polarizer. A pair of conventional 10× objectives was used as an objective and a condenser. Spectra were obtained through the $Fe^{2+/3+}$-rich and $Mn^{2+/3+}$-rich zones of the samples with the clearest areas.

Additionally, slices parallel and perpendicular to the *c* axis of Fe^{2+}-rich tourmaline crystals from Madagascar and Grasstein (sample drv18 and GRAS1, described originally by Cámara et al. 2002 and Ertl et al. 2006b, respectively) were prepared and their optical absorption spectra were recorded.

Heating and oxidation procedures

The same single crystals (~100–200 µm; details in Table 1) that were characterized structurally were placed inside a small porcelain cup (~3 cm in diameter) and heated in air by using a Nabertherm annealing furnace with programmable temperature (model N 11/H), to oxidize Fe^{2+} and Mn^{2+} of the Fe- and Mn-bearing tourmalines. Temperature was varied between 700 and 750 °C (at 1 bar) and the length of heating time was varied between 10 and 72 h (for details see section "Oxidation experiments" further below). To avoid cracks in the single crystals only relatively slow heating (100 °C/h) and cooling (100 °C/h) procedures were applied. After every heating procedure the crystals were mounted on glass fibers and subsequently characterized structurally using a CCD single-crystal diffractometer, as described in the prior section "Crystal-structure refinement." The letter "H" was added to those sample numbers that were characterized after heating.

Results

Mössbauer spectra

The Mössbauer spectra of the natural and heated/oxidized $Fe^{2+/3+}$-rich tourmaline (sample BLS) at 295 K are shown in Figures 1 and 2. Before oxidation, the spectrum (which resembles a typical tourmaline spectrum as described by Dyar et al. 1998), with ~55% of the total Fe as Fe^{2+}, ~28% in adjacent

Table 1. Crystal data, data collection information, and refinement details for natural and heat-treated Fe-rich and Mn-bearing tourmaline (BLS) from Blocherleitengraben, Lower Austria, and natural and heat-treated Mn-rich tourmaline (MNELB) from the island of Elba, Italy

Sample	BLS1	BLS2	BLS2H1	BLS2H2	MNELB3	MNELB3H
a, *c* (Å)	16.039(1), 7.254(1)	16.043(2), 7.247(1)	15.917(2), 7.252(1)	15.918(2), 7.260(1)	15.951(2), 7.138(1)	15.852(2), 7.148(1)
V (Å^3)	1612.8(3)	1615.3(4)	1591.1(4)	1593.1(4)	1572.8(4)	1555.5(4)
Crystal dimensions (mm)	0.15 × 0.15 × 0.15	0.08 × 0.10 × 0.12	0.08 × 0.10 × 0.12	0.08 × 0.10 × 0.12	0.13 × 0.17 × 0.22	0.13 × 0.17 × 0.22
Collection mode, $2\theta_{max}$ (°)	full sphere, 35.10	full sphere, 37.78	full sphere, 37.78	full sphere, 37.72	full sphere, 37.77	full sphere, 37.77
h, *k*, *l* ranges	–22/22, –22/22, –10/10	–27/27, –23/23, –12/12	–27/27, –23/23, –12/12	–27/27, –23/23, –12/12	–27/27, –23/23, –12/12	–27/27, –23/23, –12/12
Total reflections measured	3880	3855	3777	3783	3746	3713
Unique reflections	1156 (R_{int} 1.55%)	2087 (R_{int} 1.02%)	2045 (R_{int} 1.10%)	2046 (R_{int} 1.36%)	2025 (R_{int} 1.03%)	2008 (R_{int} 0.93%)
$R1(F)$, $wR2_{all}(F^2)$	1.27%, 3.33%	1.63%, 4.08%	1.60%, 4.13%	1.77%, 4.37%	1.80%, 4.82%	1.58%, 4.20%
Flack *x* parameter	0.008(10)	0.009(9)	0.031(11)	0.023(12)	–0.096(19)	–0.12(2)
"Observed" refls. [$F_o > 4\sigma(F_o)$]	1155	2055	1998	1959	2010	1988
Extinct. coefficient	0.00015(10)	0.00401(16)	0.00064(10)	0.00045(11)	0.0042(2)	0.00072(17)
No. of refined parameters	96	96	92	92	95	96
GooF	1.117	1.124	1.187	1.130	1.127	1.043
$(\Delta/\sigma)_{max}$	0.001	0.001	0.000	0.001	0.001	0.002
$\Delta\sigma_{min}$, $\Delta\sigma_{max}$ (e/Å^3)	–0.26, 0.32	–0.42, 0.45	–0.43, 0.44	–0.48, 0.44	–0.98, 0.86	–0.41, 0.37

Notes: Diffractometer: Nonius KappaCCD system except for BLS1 (Bruker Apex CCD); space group *R*3*m*; refinement on F^2. Unit-cell parameters have been refined from approximately 5500 reflections in each case.

TABLE 2. Table of positional, thermal, and occupancy parameters and their estimated standard deviations for natural and heat-treated Fe-rich and Mn-bearing tourmaline (BLS) from Blocherleitengraben, Lower Austria, and natural and heat-treated Mn-rich tourmaline (MNELB) from the island of Elba, Italy

Site	Sample	*x*	*y*	*z*	U_{eq}	Occ.
X	BLS1	0	0	0.7500(2)	0.0232(2)	$Na_{0.94(2)}Ca_{0.06}$
	BLS2	0	0	0.2214(2)	0.0233(6)	$Na_{0.94(1)}Ca_{0.06}$
	BLS2H1	0	0	0.2193(2)	0.0207(6)	$Na_{0.97(1)}Ca_{0.03}$
	BLS2H2	0	0	0.2199(2)	0.0209(6)	$Na_{0.97(1)}Ca_{0.03}$
	MNELB3	0	0	0.7714(4)	0.0239(7)	$Na_{0.666(8)}$
	MNELB3H	0	0	0.7750(3)	0.0237(5)	$Na_{0.674(7)}$
Y	BLS1	–0.12322(2)	1/2x	0.3393(2)	0.0106(1)	$Fe_{0.829(5)}Al_{0.171}$
	BLS2	0.12338(2)	1/2x	0.63190(3)	0.00889(6)	$Fe_{0.819(4)}Al_{0.189}$
	BLS2H1	0.12621(2)	1/2x	0.63391(3)	0.00985(7)	$Fe_{0.724(4)}Al_{0.276}$
	BLS2H2	0.12583(2)	1/2x	0.63456(4)	0.00990(8)	$Fe_{0.676(4)}Al_{0.324}$
	MNELB3	0.87608(2)	1/2x	0.37180(5)	0.0094(1)	$Al_{0.589(4)}Mn_{0.411}$
	MNELB3H	0.87639(2)	1/2x	0.36624(4)	0.00820(9)	$Al_{0.706(3)}Mn_{0.294}$
Z	BLS1	0.70130(3)	0.73828(2)	0.3619(2)	0.00771(9)	$Al_{0.797(3)}Fe_{0.203}$
	BLS2	0.29875(2)	0.26174(2)	0.60992(3)	0.00578(7)	$Al_{0.818(2)}Fe_{0.182}$
	BLS2H1	0.29753(2)	0.25723(2)	0.60489(4)	0.00732(7)	$Al_{0.773(2)}Fe_{0.227}$
	BLS2H2	0.29741(2)	0.25699(2)	0.60442(4)	0.00767(7)	$Al_{0.751(3)}Fe_{0.249}$
	MNELB3	0.70199(2)	0.73879(2)	0.38810(4)	0.00538(6)	$Al_{1.00}$
	MNELB3H	0.70324(2)	0.74109(2)	0.39232(3)	0.00685(7)	$Al_{0.935(3)}Mn_{0.065}$
B	BLS1	0.88976(7)	2x	0.5194(3)	0.0102(3)	$B_{1.00}$
	BLS2	0.11031(5)	2x	0.4529(2)	0.0080(2)	$B_{1.00}$
	BLS2H1	0.11019(6)	2x	0.4533(2)	0.0071(2)	$B_{1.00}$
	BLS2H2	0.11011(6)	2x	0.4532(3)	0.0079(3)	$B_{1.00}$
	MNELB3	0.89002(5)	2x	0.5443(2)	0.0065(2)	$B_{1.00}$
	MNELB3H	0.89009(4)	2x	0.5463(2)	0.0066(2)	$B_{1.00}$
T	BLS1	0.80868(2)	0.81039(2)	0.9732(2)	0.0076(1)	$Si_{1.00}$
	BLS2	0.19142(2)	0.18967(2)	–0.00132(4)	0.00569(6)	$Si_{1.00}$
	BLS2H1	0.19113(2)	0.19027(2)	0.00136(4)	0.00554(6)	$Si_{1.00}$
	BLS2H2	0.19105(2)	0.19018(2)	0.00121(4)	0.00590(7)	$Si_{1.00}$
	MNELB3	0.80813(2)	0.81005(2)	0.99836(4)	0.00493(5)	$Si_{1.00}$
	MNELB3H	0.80860(1)	0.81006(1)	0.99750(3)	0.00519(5)	$Si_{1.00}$
H3	BLS1	–0.270(4)	1/2x	0.583(6)	0.08(2)	$H_{1.00}$
	BLS2	0.260(3)	1/2x	0.381(6)	0.06(1)	$H_{1.00}$*
	MNELB3	0.738(3)	1/2x	0.609(5)	0.029(9)	$H_{1.00}$
	MNELB3H	0.751(3)	1/2x	0.622(6)	0.08(1)	$H_{1.00}$†
O1	BLS1	0	0	0.1945(3)	0.0219(5)	$O_{0.70(5)}F_{0.30}$
	BLS2	0	0	0.7819(3)	0.0237(6)	$O_{0.70(5)}F_{0.30}$
	BLS2H1	0	0	0.7643(3)	0.0102(3)	$O_{1.00}$
	BLS2H2	0	0	0.7627(3)	0.0100(3)	$O_{1.00}$
	MNELB3	0	0	0.2193(4)	0.045(1)	$O_{0.43(7)}F_{0.57}$
	MNELB3H	0	0	0.2363(2)	0.0150(4)	$O_{0.86(4)}F_{0.14}$
O2	BLS1	0.93852(5)	2x	0.4919(3)	0.0144(3)	$O_{1.00}$
	BLS2	0.06156(4)	2x	0.4800(2)	0.0127(2)	$O_{1.00}$
	BLS2H1	0.06080(4)	2x	0.4850(2)	0.0095(2)	$O_{1.00}$
	BLS2H2	0.06072(4)	2x	0.4857(2)	0.0100(2)	$O_{1.00}$
	MNELB3	0.93850(4)	2x	0.5136(2)	0.0180(3)	$O_{1.00}$
	MNELB3H	0.93913(3)	2x	0.5110(1)	0.0115(2)	$O_{1.00}$
O3	BLS1	–0.2668(1)	1/2x	0.4614(3)	0.0171(3)	$O_{1.00}$
	BLS2	0.2678(1)	1/2x	0.5101(2)	0.0148(2)	$O_{1.00}$
	BLS2H1	0.26034(9)	1/2x	0.5224(2)	0.0105(2)	$O_{1.00}$
	BLS2H2	0.25949(9)	1/2x	0.5225(2)	0.0109(2)	$O_{1.00}$
	MNELB3	0.7320(1)	1/2x	0.4892(2)	0.0118(2)	$O_{1.00}$
	MNELB3H	0.74050(7)	1/2x	0.4849(1)	0.0117(1)	$O_{1.00}$
O4	BLS1	0.90743(5)	2x	0.9047(3)	0.0130(3)	$O_{1.00}$
	BLS2	0.09269(4)	2x	0.0675(2)	0.0107(2)	$O_{1.00}$
	BLS2H1	0.09408(4)	2x	0.0776(2)	0.0097(2)	$O_{1.00}$
	BLS2H2	0.09423(5)	2x	0.0779(2)	0.0102(2)	$O_{1.00}$
	MNELB3	0.90643(4)	2x	0.9285(2)	0.0091(2)	$O_{1.00}$
	MNELB3H	0.90523(3)	2x	0.9222(1)	0.0098(1)	$O_{1.00}$
O5	BLS1	–0.1846(1)	1/2x	0.8840(3)	0.0130(2)	$O_{1.00}$
	BLS2	0.18477(8)	1/2x	0.0879(2)	0.0106(2)	$O_{1.00}$
	BLS2H1	0.18202(9)	1/2x	0.0853(2)	0.0102(2)	$O_{1.00}$
	BLS2H2	0.18185(9)	1/2x	0.0853(2)	0.0106(2)	$O_{1.00}$
	MNELB3	0.81260(8)	1/2x	0.9066(2)	0.0095(2)	$O_{1.00}$
	MNELB3H	0.81440(7)	1/2x	0.9073(1)	0.0107(1)	$O_{1.00}$
O6	BLS1	0.80337(7)	0.81272(7)	0.1945(3)	0.0116(2)	$O_{1.00}$
	BLS2	0.19673(5)	0.18745(6)	0.7771(1)	0.0095(1)	$O_{1.00}$
	BLS2H1	0.19188(5)	0.18634(6)	0.7789(1)	0.0085(1)	$O_{1.00}$
	BLS2H2	0.19142(6)	0.18593(6)	0.7787(1)	0.0089(1)	$O_{1.00}$
	MNELB3	0.80269(5)	0.81281(6)	0.2233(1)	0.0081(1)	$O_{1.00}$
	MNELB3H	0.80696(4)	0.81508(4)	0.22339(8)	0.00814(9)	$O_{1.00}$
O7	BLS1	0.71602(7)	0.71574(6)	0.8939(3)	0.0123(2)	$O_{1.00}$
	BLS2	0.28411(5)	0.28447(5)	0.0780(1)	0.0100(1)	$O_{1.00}$
	BLS2H1	0.28586(6)	0.28515(5)	0.0767(1)	0.0086(2)	$O_{1.00}$
	BLS2H2	0.28587(6)	0.28509(6)	0.0763(1)	0.0090(1)	$O_{1.00}$
	MNELB3	0.71441(5)	0.71398(5)	0.9192(1)	0.0072(1)	$O_{1.00}$
	MNELB3H	0.71347(4)	0.71388(4)	0.92205(7)	0.00740(9)	$O_{1.00}$
O8	BLS1	0.79074(7)	0.72986(8)	0.5317(3)	0.0150(2)	$O_{1.00}$
	BLS2	0.20933(6)	0.27023(6)	0.4403(1)	0.0123(1)	$O_{1.00}$
	BLS2H1	0.20932(6)	0.27020(6)	0.4402(1)	0.0091(1)	$O_{1.00}$
	BLS2H2	0.20918(6)	0.26999(6)	0.4395(1)	0.0099(2)	$O_{1.00}$
	MNELB3	0.79000(5)	0.72921(6)	0.5579(1)	0.0085(1)	$O_{1.00}$
	MMELB3H	0.79026(4)	0.72920(4)	0.56059(8)	0.00797(9)	$O_{1.00}$

Note: For definition of U_{eq} see Fischer and Tillmanns (1988).
* In BLS2H1 and BLS2H2, the H site was not detected.
† See text for discussion of the H site in MNELB3H.

Y and *Z* sites shared between Fe^{2+} and Fe^{3+}, and ~17% as Fe^{3+}. The Mössbauer spectra of the Fe^{2+}-rich tourmaline sample were fit to a total of four distributions with the Mössbauer parameters (Table 5) consistent with those reported by Dyar et al. (1998). The outermost two doublets (gray dashed lines in Fig. 1) have parameters corresponding to octahedral Fe^{2+}, although the Mössbauer results alone cannot distinguish occupancy of the *Y* vs. the *Z* site. The third doublet (solid gray line), which has an isomer shift (IS) of 0.93 mm/s, lies in the range for electron delocalized (ED) peaks, sharing an electron between Fe^{2+} and Fe^{3+} between adjacent octahedral sites. Thus, the area of the doublet must be considered to be the proportion of Fe that is ephemeral between the two valence states. Finally, the last doublet, with an isomer shift of 0.44 mm/s, represents Fe^{3+} in octahedral coordination; again, a nonspecific site assignment between the *Y* or *Z* site. After oxidation 100% of the Fe is oxidized to Fe^{3+} in an octahedral site as indicated by a Mössbauer study (Table 5, Fig. 2).

Optical spectra

The optical spectrum of the Blocherleitengraben Fe^{2+}-rich tourmaline (Fig. 3a) is comparable to that of the high Fe-content tourmalines that contain both Fe^{2+} and Fe^{3+} discussed in Mattson and Rossman (1987). The spectrum contains Fe^{2+} bands near 720 and 1120 nm in the E*c* polarization. In E⊥c, even at 32 µm thickness, intense absorption is encountered across the visible and much of the near-infrared portion of the spectrum due to the interaction of Fe^{2+} with Fe^{3+}. Such an intensity difference between the E*c* and E⊥*c* directions indicates that an Fe^{2+}-Fe^{3+} interaction is occurring between adjacent sites (Mattson and Rossman 1987). There are also weak indications in the E*c* polarization of a Fe^{2+}-Ti^{4+} intervalence charge transfer band near 420 nm, a Mn^{3+} band near 530 nm, and an overtone of the OH band near 1420 nm. The heated Fe^{3+}-rich tourmaline (BLS2H2, see below for details) shows a nearly complete loss of Fe^{2+} bands (Fig. 3b).

The optical spectra of the Mn^{2+}-rich (unheated) tourmaline from Elba reflect the variation in color from yellow at one end of the whole crystal to a darker yellow-brown at the other. The spectrum of the yellow region is nearly devoid of features (Fig. 4) except for the OH overtone bands near 1430 nm in the E*c* orientation and the rising absorption in the short wavelength region that is more intense in the E⊥*c* spectrum. There is also a weak, sharp, spin-forbidden Mn^{2+} feature near 415 nm, barely

visible at the scale of Figure 4 of the unheated sample (not visible in the heated sample).

In the spectrum (not shown) of the darker portion of the (unheated) Elba crystal, the Fe^{2+} features near 720 and 1120 nm are prominent. The intensity of the two Fe^{2+} bands in the E⊥*c* polarization is about twice the intensity of the E*c* bands, indicating that some Fe^{2+}-Fe^{3+} interaction is occurring in the darker region. The darker region also has a broad band near 420 nm typical of Fe^{2+}-Ti^{4+} intervalence charge transfer (Mattson and Rossman 1988).

The optical absorption spectra (Figs. 5 and 6) of additional Fe^{2+}-rich tourmaline crystals from Madagascar and Grasstein (sample drv18 and GRAS1, described originally by Cámara et al. 2002 and Ertl et al. 2006b, respectively), show a pair of bands corresponding to Fe^{2+} at about 770 and 1160 nm in the E\\c polarization.

Crystal chemistry and structure analysis

Fe^{2+}-rich tourmaline. The pegmatitic Fe^{2+}-rich tourmaline (chemical composition see Table 4) from Blocherleitengraben, Lower Austria (BLS1) has elevated contents of Fe_{total} (3.26 apfu Fe_{total}; 2.25 apfu Fe^{2+}, 1.01 apfu Fe^{3+}) and significant amounts of the larger Mn^{2+} (0.32 apfu). This is reflected in the <*Y*-O> distance of 2.063 Å (Table 3), which is the longest observed in tourmaline to date. The longest <*Y*-O> distance so far with 2.060 Å was observed in a schorl from the St. Andreasberg District, Harz Mts., Lower Saxony, Germany, by Fortier and Donnay (1975). The Fe occupancy determined from the high-quality structural refinement (R = 1.27%) is in very good agreement with the chemical data. The *X*-site occupancy, as determined by chemical analysis (11.4 e^-), is in good agreement with the refined occupancy [11.5(2) e^-]. The sum of *Y*- and *Z*-site occupancy (164.8 e^-) shows very good agreement (difference: ~0.2%) with the sum of the refined occupancies (165.2 e^-). Because of this excellent agreement between chemical and structural data we are able to address the site occupations very accurately. The calculated water content of 2.70 wt% is consistent with the water content of 2.6(1) wt% as determined by TGA. The *W* site has a slightly greater amount of monovalent anions (F^{1-} + OH^{1-} = 0.51 apfu) than divalent anions (O^{2-} = 0.49 apfu). In accordance with the dominant valency rule (Hatert and Burke 2008; Henry

TABLE 3. Selected interatomic distances (Å) in natural and heat-treated Fe-rich and Mn-bearing tourmaline (BLS) from Blocherleitengraben, Lower Austria, and natural and heat-treated Mn-rich tourmaline (MNELB) from the island of Elba, Italy

	BLS1	BLS2	BLS2H1	BLS2H2	MNELB3	MNELB3H
X-O2 (x3)	2.534(2)	2.537(2)	2.554(2)	2.555(2)	2.504(2)	2.521(2)
X-O5 (x3)	2.742(2)	2.743(2)	2.691(1)	2.691(1)	2.763(2)	2.718(1)
X-O4 (x3)	2.806(2)	2.807(1)	2.790(1)	2.795(1)	2.818(2)	2.807(1)
Mean	2.694	2.696	2.678	2.680	2.695	2.682
Y-O1	2.027(2)	2.030(3)	1.980(1)	1.968(1)	2.029(2)	1.9347(9)
Y-O2 (x2)	2.037(1)	2.0358(8)	2.0215(8)	2.0189(8)	1.9833(9)	1.9766(6)
Y-O6 (x2)	2.044(1)	2.0466(8)	1.9986(8)	1.9937(9)	2.0361(8)	1.9785(7)
Y-O3	2.182(2)	2.192(1)	2.018(1)	2.014(1)	2.160(1)	2.049(1)
Mean	2.062	2.064	2.006	2.001	2.038	1.982
Z-O6	1.904(1)	1.9018(8)	1.9481(8)	1.9540(9)	1.8604(8)	1.8996(6)
Z-O8	1.905(1)	1.9037(8)	1.9111(8)	1.9137(9)	1.8840(8)	1.8900(6)
Z-O7	1.911(1)	1.9075(8)	1.9088(8)	1.9127(9)	1.8789(8)	1.8884(6)
Z-O8′	1.946(1)	1.9449(9)	1.9314(8)	1.9337(9)	1.9178(8)	1.9092(6)
Z-O7′	1.986(1)	1.9845(8)	2.0226(9)	2.0261(9)	1.9561(8)	1.9692(6)
Z-O3	1.9913(7)	1.9895(6)	1.8978(6)	1.8968(6)	1.9739(6)	1.9416(5)
Mean	1.941	1.939	1.937	1.940	1.912	1.916
T-O7	1.6087(9)	1.6105(8)	1.6050(8)	1.6054(8)	1.6161(7)	1.6095(6)
T-O6	1.609(1)	1.6093(9)	1.6152(8)	1.6171(9)	1.6098(8)	1.6174(6)
T-O4	1.6270(5)	1.6288(5)	1.6253(5)	1.6259(5)	1.6245(5)	1.6208(4)
T-O5	1.6425(6)	1.6429(5)	1.6305(5)	1.6305(6)	1.6376(5)	1.6291(4)
Mean	1.622	1.623	1.619	1.620	1.622	1.619
B-O2	1.369(3)	1.369(2)	1.381(2)	1.382(2)	1.357(2)	1.370(2)
B-O8 (x2)	1.378(2)	1.379(1)	1.370(1)	1.369(1)	1.385(1)	1.3744(8)
Mean	1.375	1.376	1.374	1.373	1.376	1.373

TABLE 4. Composition of Fe-rich and Mn-bearing tourmaline from Blocherleitengraben, Lower Austria, and of a Mn-rich tourmaline from the island of Elba, Italy (wt%)

	BLS1*	MNELB3†
SiO_2	32.99(23)	36.37(19)
TiO_2	1.06(3)	0.22(1)
B_2O_3	9.68‡	10.54‡
Al_2O_3	25.10(11)	37.05(14)
Cr_2O_3	0.01(1)	b.d.
FeO_{total}	21.66(22)	0.09(2)
FeO§	14.95	–
Fe_2O_3§	7.46	–
MnO‖	2.13(7)	9.28(13)
MgO	0.09(2)	b.d.
CaO	0.38(2)	0.04(1)
Li_2O	0.00#	0.70**
ZnO	0.17(3)	b.d.
Na_2O	2.51(7)	1.98(6)
K_2O	0.09(1)	b.d.
F	0.49(3)	0.98(12)
H_2O	2.70††	2.76††
O≡F	–0.21	–0.41
Sum	99.60	99.60
n	31	31
Si	5.92	6.00
$^{[4]}$Al	0.08	–
Sum *T* site	6.00	6.00
$^{[3]}$B	3.00	3.00
Al	5.23	7.20
Mn^{2+}	0.32	1.30
Fe^{2+}	2.25	0.01
Fe^{3+}	1.01	–
Mg	0.03	–
Li	–	0.46
Zn	0.02	–
Ti^{4+}	0.14	0.03
Sum *Y, Z* sites	9.00	9.00
Na	0.88	0.63
Ca	0.07	0.01
K	0.02	–
	0.03	0.36
Sum *X* site	1.00	1.00
Sum cations	18.97	18.55
OH	3.23	3.04
F	0.28	0.51
Sum OH + F	3.51	3.55

* Average of 8 EMP analyses. Standard deviation in brackets.
† Average of 10 EMP analyses. Uncertainty (wt%) for Li_2O and H_2O: 0.11 and 0.05 respectively.
‡ Calculated for B = 3.00 apfu, because there is no structural evidence for significant amounts of $^{[4]}$B (<*T*-O> distances >1.620 Å).
§ FeO and Fe_2O_3 were determined by Mössbauer spectroscopy (Table 6).
‖ Total Mn calculated as MnO. For details about the valence state of Mn in these samples see text. Cl is below the detection limit.
The Li content (33 ppm) was determined by ICP-MS.
** H_2O content calculated based on charge balance assuming a normalization of $Y + Z + T$ = 15.00 apfu. These values are consistent with the measured water contents of 2.6(2) wt% (BLS1) and 3.0(2) wt% (MNELB3) as determined by TGA.
b.d.: below detection limit.
†† Determined by flame AAS.

et al. 2011), the dominant anion of the dominant valency on a site becomes the basis for naming the species. Because F^{1-} (0.28 apfu) is greater than $(OH)^{1-}$ (0.23 apfu) this tourmaline is a fluor-schorl. However, the chemical composition of this sample shows that it belongs either to a schorl, fluor-schorl, or to an oxy-schorl (Bačik et al. 2011b) within the analytical errors. This sample breaks down (to hematite and mullite; consistent with oxidation experiments by Bačik et al. 2011a) at ~950 °C in air (onset: 920 °C, endset: 970 °C), and in N_2 at ~860 °C (onset: 840 °C, endset: 910 °C).

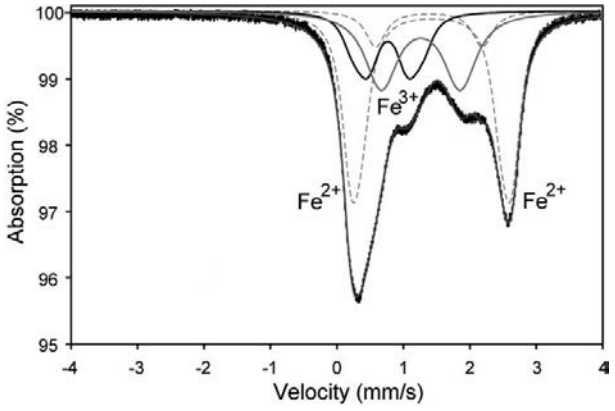

FIGURE 1. Room-temperature (295 K) Mössbauer spectrum of Fe-rich tourmaline from Blocherleitengraben, Lower Austria (sample BLS).

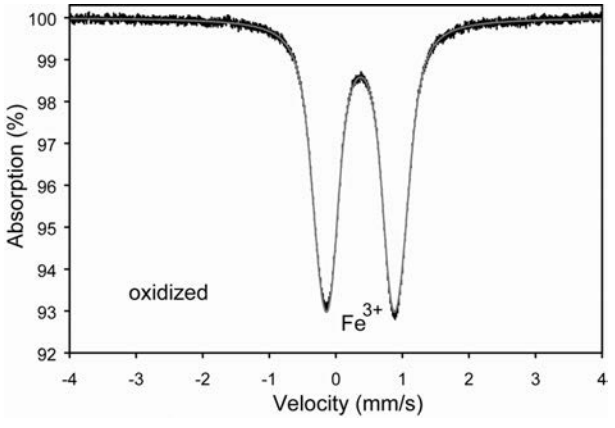

FIGURE 2. Room-temperature (295 K) Mössbauer spectrum of Fe-rich tourmaline from Blocherleitengraben, Lower Austria, which was heated and oxidized at 750 °C for 60 h (sample BLSH).

TABLE 5. Mössbauer parameters for Fe-rich tourmaline (sample BLS) from Blocherleitengraben, Lower Austria

	CS (mm/s)	QS (mm/s)	% Area
BLS (natural)			
Fe^{2+}	1.09	2.43	46.5
Fe^{2+}	1.06	1.58	8.5
ED Fe^{2+}-Fe^{3+}	0.93	1.17	28
Fe^{3+}	0.44	0.59	17
BLSH (oxidized)			
Fe^{3+}	0.37	0.95	100

Notes: Results are given in mm/s relative to the center point of a Fe-foil calibration spectrum. The Lorentzian full peak width (γ) at half maximum intensity is held constant at 0.20 mm/s. CS: the value of isomer shift, when the distributed hyperfine parameter has a value of zero. QS: the center of a Gaussian component of the Δ-distribution. % Area = the relative area of doublet. The ratio of Lorentzian heights of the two lines in an elemental quadrupole doublet, h_+/h_-,was constrained to have a value of 1 for all sub-components.

Based strictly on the structure refinements (and considering the associated error) the *Z*-site occupancy in BLS1 is determined to be $^{Z}(Al_{4.78}Fe_{1.22})$, reflecting ~37% of the total Fe at the *Z* site. By including the uncertainty in the Fe^{3+} determination by Mössbauer spectroscopy, the range of Fe^{3+} in this sample is ~26–36% (~31 ± 5%) of the total Fe. The amount of Fe^{3+} is the sum of ~17% $^{[6]}Fe^{3+}$ and ~14% $^{[6]}Fe^{3+}$ that arises from the time-averaged iron involved in the intervalence interaction (~28% Fe^{2+}-Fe^{3+} ED; Table 5). Furthermore, by taking into account the errors of the chemical and Mössbauer analyses, the total estimated amount of Fe^{3+} is approximately consistent with the amount of Fe at the *Z* site determined from structure refinement. However, by taking into consideration the errors of the structure refinement (3σ) and the Mössbauer data and accepting that Ti^{4+} (which has a smaller effective ionic radius than Fe^{3+}; $^{[6]}Ti^{4+}$: 0.605 Å; $^{[6]}Fe^{3+}$: 0.645 Å; Shannon 1976) could occupy the *Z* site and that there are delocalized electrons that are hopping between the *Y* site and the *Z* site, and maybe also between the *Y* sites, we propose two different formulas in the following section.

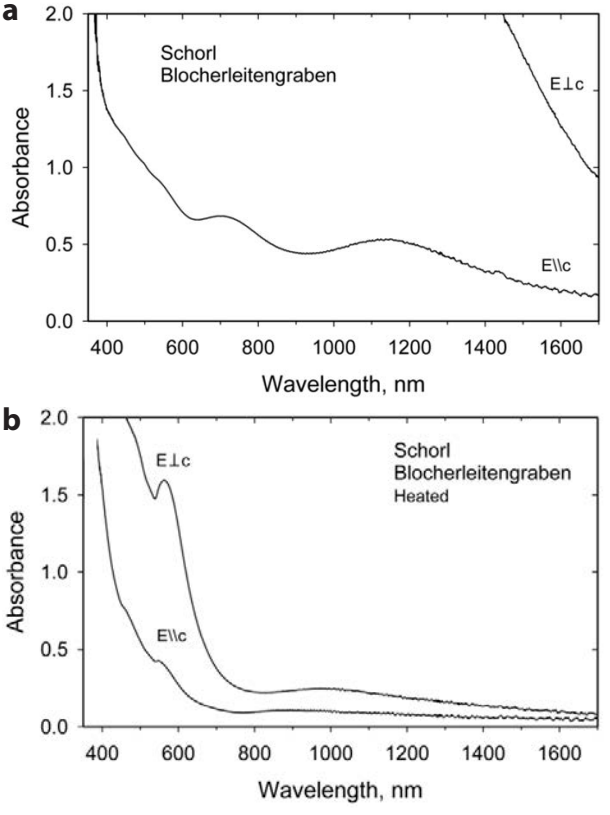

FIGURE 3. (**a**) Optical absorption spectra of a 30 μm thick thin-sections of unheated Fe^{2+}-rich tourmaline from Blocherleitengraben, Lower Austria (sample BLS). Weak OH overtone bands can be seen near 1430 nm in the E*c* direction. (**b**) Optical absorption spectra of a 30 μm thick thin-section of Fe^{3+}-rich tourmaline from Blocherleitengraben, Lower Austria (sample BLS), which show the dramatic loss of intensity of the Fe^{2+} bands in the E⊥*c* direction after oxidation (heating at 750 °C/60 h).

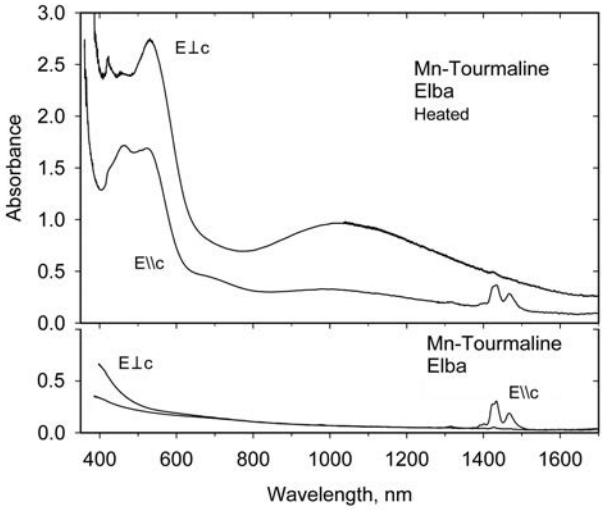

FIGURE 4. Optical absorption spectra of a 0.637 mm thick crystal plate of Mn-rich tourmaline from Elba Island, Italy (sample MNELB3) in its original unheated state (**bottom**) and after heating (**top**) to 750 °C for 30 h.

A brief note on the assignment of Ti^{4+} to the *Z* site that is strongly supported by calculation of bond-valence sums for the ion in the two octahedral sites. In the two unheated samples (BLS1, BLS2) Ti^{4+} is greatly underbonded in the *Y* site (3.11 and 3.09 v.u., respectively), but near its formal valence in the *Z* sites (4.29 and 4.32 v.u., respectively). In the heated samples (BLS2H1, BLS2H2), Ti bond valence sums are still closer to the formal valence at the *Z* site (4.35 and 4.31 v.u., respectively), but the *Y* site bond-valence sums are much closer to the formal valence (3.58 and 3.63 v.u., respectively) than in the unheated sample.

On basis of the chemical data, the structural refinement, and the Mössbauer data, the first proposed formula was determined by assigning all of the Fe^{3+} (the amount of Fe^{2+} and Fe^{3+} from the *Y*-*Z* ED doublet were assigned to the *Y* and *Z* site) and Ti^{4+} to the *Z* site: $^{X}(Na_{0.88}Ca_{0.07}K_{0.02}\square_{0.03})$ $^{Y}(Fe^{2+}_{2.02}Al_{0.41}Mn^{2+}_{0.32}Fe^{3+}_{0.23}Zn_{0.02})$ $^{Z}(Al_{4.82}Fe^{3+}_{0.78}Fe^{2+}_{0.23}Ti^{4+}_{0.14}Mg_{0.03})$ $^{T}(Si_{5.92}Al_{0.08})O_{18}$ $(BO_3)_3$ $^{V}(OH)_3$ $^{W}[O_{0.49}F_{0.28}(OH)_{0.23}]$. The assigned *Y*-site occupants gives 24.1 e⁻/site, which is in excellent agreement with the refined occupancy of 23.8(1) e⁻. The assigned *Z*-site occupants yield 15.4 e⁻/site, again in excellent agreement with the refined occupancy of 15.6(1) e⁻. This first formula supports the lack of Fe^{2+} at the *Z* site, apart from that connected with delocalization of a hopping electron. Such an assignment is also in accord with the bond-valence sums calculated for Fe^{2+} at the *Y* and *Z* sites. The calculated bond-valence sum for Fe^{2+} at the *Y* site ranges between 2.39 and 3.06 v.u. for the analyzed tourmalines (for which spectroscopic measurements were also performed), whereas it is significantly overbonded at the *Z* site, with bond-valence sums that range between 3.39 and 3.74 v.u.

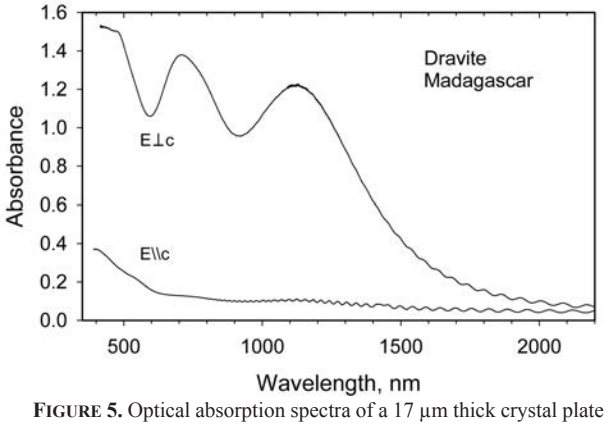

FIGURE 5. Optical absorption spectra of a 17 µm thick crystal plate of Fe-rich dravite from Madagascar (sample drv18, no. 108796; Dyar et al. 1998, 2001). The sinusoidal features at longer wavelengths are interference fringes that arise from the thinness of the sample.

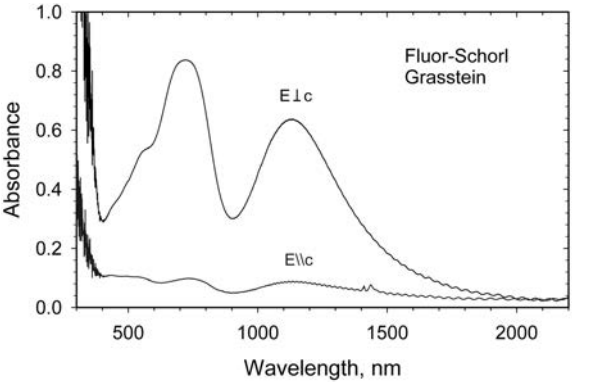

FIGURE 6. Optical absorption spectra of a 45 µm thick crystal plate of fluor-schorl from Grasstein, South Tyrol, Italy (sample GRAS1 from Ertl et al. 2006b).

For a second proposed formula, both ED doublets (*Y*-*Z* and *Y*-*Y*) were considered: $^{X}(Na_{0.88}Ca_{0.07}K_{0.02}\square_{0.03})$ $^{Y}(Fe^{2+}_{1.84}Al_{0.48}Mn^{2+}_{0.32}Fe^{3+}_{0.34}Zn_{0.02})$ $^{Z}(Al_{4.75}Fe^{3+}_{0.67}Fe^{2+}_{0.41}Ti^{4+}_{0.14}Mg_{0.03})$ $^{T}(Si_{5.92}Al_{0.08})O_{18}$ $(BO_3)_3$ $^{V}(OH)_3$ $^{W}[O_{0.49}F_{0.28}(OH)_{0.23}]$. The assigned *Y*-site occupants give 23.8 e⁻/site, which match the refined occupancy. The assigned *Z*-site occupants yield 15.5 e⁻/site, in excellent agreement with the refined occupancy [15.6(1) e⁻/site]. This second formula requires some Fe^{2+} (~0.3 apfu) at the *Z* site, apart from that connected with delocalization of a hopping electron.

To check if there is any spectroscopic evidence for $^{Z}Fe^{2+}$ in two other Fe^{2+}-rich tourmalines (sample drv18 and GRAS1, described originally by Cámara et al. 2002 and Ertl et al. 2006b, respectively), their optical absorption spectra (Figs. 5 and 6) were recorded. If Fe^{2+} were to occupy two different 6-coordinated sites in significant amounts (e.g., samples drv18 and GRAS1: ~^{Y}0.4–1.6 apfu Fe^{2+} and ~^{Z}0.4–0.6 apfu Fe^{2+} as proposed by Bosi 2008) and if these polyhedra have different geometries or metal-oxygen distances, bands from each site should be observed in the spectrum, most likely in the 1160 nm region in the E*c* polarization. However, even in high-quality spectra we see no evidence for a doubling of the bands. When we consider the samples described by Bosi et al. (2008) and Bosi and Lucchesi (2007), we note that various amounts of Fe have been found at the *Z* site by X-ray refinement. We further note that there is always enough Fe^{3+} in the Mössbauer spectrum to fully account for all of the Fe at the *Z* site. Bosi (2008) and Bosi and Lucchesi (2007) assigned to the *Y* site, to occupy the *Z* site in the same amount. Furthermore, the authors of the present study are

not aware of any reference where the structure refinement of a $Fe^{2+/3+}$-rich tourmaline shows significantly more Fe at the *Z* site than the total amount of Fe^{3+} estimated by a Mössbauer study (in combination with chemical analysis).

Mn^{2+}-rich tourmaline. The most Mn^{2+}-rich sample, with a similar Mn^{2+} content as the Mn^{2+}-rich samples from Elba published by Bosi et al. (2005a), was subsequently characterized chemically. The portion of this crystal richest in Mn^{2+} (and with dark yellow color), which was separated and characterized structurally and chemically (including the estimation of the OH content), has the structural formula $^{X}(Na_{0.63}Ca_{0.01}\square_{0.36})$ $^{Y}(Mn^{2+}_{1.30}Al_{1.20}Li_{0.46}Ti^{4+}_{0.03}Fe^{2+}_{0.01})$ $^{Z}Al_6$ $^{T}Si_6O_{18}$ $(BO_3)_3$ $^{V}(OH)_3$ $^{W}[F_{0.51}O_{0.45}(OH)_{0.04}]$ (sample MNELB3; Tables 1–4). This tourmaline is the F-analog of tsilaisite (Bosi et al. 2011). The unit-cell parameters of MNELB3 [a = 15.951(2) and c = 7.138(1) Å, Table 2] are very similar to, or even higher than those from the Mn^{2+}-richest samples from Bosi et al. (2005a) [a = 15.9398(6)–15.9461(5) Å and c = 7.1363(3)–7.1380(3) Å]. This tourmaline breaks down (mainly to mullite) at ~920 °C in N_2 (onset: 910 °C, endset: 935 °C). A refinement of the Al:Mn ratio on the *Z* site gave 5.95:0.05(2). Thus, within a 3σ error there is no clear evidence for Mn at the *Z* site.

To determine if the refinement procedures of Mn^{2+}-rich tourmalines from Austria (Ertl et al. 2003) can be modified to indicate possible Mn^{2+} at the *Z* site, we removed the restrictions of the occupancy of the *Z* site (constrained at full occupancy), while maintaining the *T* site and the B site at full occupancy ($Si_{1.00}$, $B_{1.00}$). However, even in the most Mn-rich tourmaline sample {sample BT with formula $\sim^{X}(Na_{0.8}\square_{0.2})$ $^{Y}(Al_{1.3}Mn^{2+}_{1.2}Li_{0.4}\square_{0.1})$ $^{Z}Al_6$ $^{T}(Si_{5.8}Al_{0.2})O_{18}$ $(BO_3)_3$ $^{V}(OH)_3$ $^{W}[F_{0.4}O_{0.3}(OH)_{0.3}]$; MnO: ~9 wt%}, the unconstrained occupancy decreased slightly to $Al_{0.996(3)}$ (equal to ~5.98(2) apfu Al at the *Z* site). Thus, the *Z* site is, within a 3σ error, solely occupied by Al. Hence, in the Austrian Mn^{2+}-rich tourmaline there is no clear evidence that significant amounts of Mn^{2+} or Mn^{3+} occupy the *Z* site.

Oxidation experiments

Fe^{3+}-rich tourmaline. Sample BLS2 (extracted from near the core of the Fe^{2+}-rich tourmaline crystal from Blocherleitengraben) was heated in air at 700 °C for 10 h (BLS2H1). The <*Y*-O> distance was significantly smaller (2.006 Å) than before heating (2.064 Å), which is consistent with the oxidation of a large amount of Fe^{2+} (Table 3). Although the <*Z*-O> distance did not change significantly after heating, the refined ^{Z}Fe content was larger than before heating (Table 2). Simultaneously the refined ^{Y}Fe content was smaller than before heating (decrease by 11.6%). The same observations were made after heating BLS2H1 a second time at 750 °C for 72 h (BLS2H2; Table 2). After the second heat-treatment, in this sample we found ~2.03 apfu ^{Y}Fe and ~1.49 apfu ^{Z}Fe by refinement (Table 2). The untreated single crystal had, before any heating, ~2.46 apfu ^{Y}Fe and ~1.09 apfu ^{Z}Fe (Table 2). These observations can be explained by a distinct Fe ↔ Al exchange between the *Y* and *Z* sites during oxidation. During this process, H was fully expelled, probably as H_2O, because no H was found near O3 by refinement in the heated samples BLS2H1 and BLS2H2, and the minor amount of F (at the O1 site) was replaced by O completely (within error limits of the structure refinement; results in Table 2). The unit-cell parameter *a* decreased during the first heating step, but did not change any further after the second heating step (Table 1). In contrast, the *c* parameter showed a slight increase after both heating steps, resulting in a slight net volume increase during the second heating. The final product was a conversion of the tourmaline to one with a buergerite composition with approximately all Fe^{2+} oxidized to Fe^{3+} {Table 5, Figs. 2–3, structural formula of BLS2H2: $\sim^{X}(Na_{0.9}Ca_{0.1})$ $^{Y}(Fe^{3+}_{1.6}Al_{1.0}Mn^{3+}_{0.2}Ti^{4+}_{0.1})$ $^{Z}(Al_{4.3}Fe^{3+}_{1.7})$ $^{T}(Si_{5.9}Al_{0.1})O_{18}$ $(BO_3)_3$ $^{V}[O_2(OH)]$ ^{W}O}. The Fe^{2+} absorption bands at 710 nm and 1130 nm region in the E*c* direction of the optical spectrum (Fig. 3b) disappeared as a result of the heating process as did the overtones of the OH stretching bands near 1430 nm. Likewise, the very intense Fe^{2+} bands enhanced by interaction with Fe^{3+} in the E⊥*c* direction also vanished after heating. The most prominent remaining features in the spectrum, bands near 1130 and 580 nm, are assumed to arise from Mn^{3+}. Their positions, relative intensity, polarizations, and shape mimic the corresponding Mn^{3+} features seen in the heated Elba tourmaline as well as those in common, naturally pink elbaites. Upon heating, the previously blackish crystal fragment became brown-red; the transparency was unchanged.

Mn^{3+}-rich tourmaline. Similar effects were observed during heating of the Mn-rich tourmaline. After heating of MNELB3 at 750 °C for 30 h (sample MNELB3H) the <*Y*-O> distance decreased from 2.038 to 1.982 Å (Table 2). Some Mn^{2+} of the *Y* site was exchanged during oxidation to Mn^{3+} with some Al of the *Z* site ($^{Z}Al \leftrightarrow {}^{Z}Mn^{3+}$). Before heating ~1.23 apfu ^{Y}Mn (no clear evidence for Mn at the *Z* site) was found by refinement. After heating ~0.88 apfu ^{Y}Mn and ~0.39 apfu ^{Z}Mn were found by refinement (Table 2). We suspect that a significant amount of H (at the O3 site) was lost during oxidation of some Mn^{2+} to Mn^{3+} as was indicated by an increased U_{eq} of the H atom (~0.03 → ~0.08 Å^2) in sample MNELB3H (Table 2). Moreover, the F content [0.57(7) F apfu according to refinement] decreased considerably [0.14(4) apfu after heating] indicating that evolved F was exchanged with O. The unit-cell parameter *a* decreased during heating whereas the *c* parameter showed a slight increase (Table 1). After heating at 750 °C for 30 h, the dark yellow sample was dark brown-red, with unchanged transparency (Fig. 7), as expected for the oxidation of Mn^{2+} to Mn^{3+}. The visible-NIR absorption spectrum (Fig. 4) of the heated sample showed broad bands near 532 and ~1040 nm, which are due to Mn^{3+}. The remaining brown component of the red color arises from residual Mn^{2+} as evidenced by the sharp, spin-forbidden band at 421 nm. Interestingly, the sharp band in the unheated sample (Fig. 4) that corresponds to the spin-forbidden transition of Mn^{2+} occurs at 415 nm, as previously observed in Mn-rich tourmalines from the Lundazi District of Zambia by Mattson and Rossman (1986). The shift in band position is not fully understood but probably originates from the exchange of Mn from the *Y* to the *Z* site. The integrated intensity of the OH overtone bands can be seen near 1430 nm in the spectra of both the heated and unheated samples but decreases in the spectrum of the heated sample (Fig. 4), consistent with the interpretation of the amount of H from the single-crystal refinements.

DISCUSSION

Mössbauer spectra

To determine the abundance of Fe^{3+} in the unheated Fe^{2+}-rich tourmaline, it is necessary to assign half of the electron delocalized Fe to Fe^{3+} and half to Fe^{2+}. On the basis of these data, we can conclude that this sample contains 17% of the total Fe in the Fe^{3+} doublet, 28% in the ED doublet, of which half—or 14%—can be assigned to Fe^{3+}, and thus ~31% of the total Fe as Fe^{3+}.

The correspondence between specific sets of isomer shift and quadrupole splitting and a site assignment must always be based on analogous Mössbauer measurements of minerals with known Mössbauer parameters for similar sites or, fundamentally, on corroborating single-crystal structure refinements on the same samples. Assignment of the Fe^{2+} doublets to *Y* sites in the Dyar et al. (1998) paper was mainly based on the compelling theoretical models of Pieczka (1997), Pieczka and Kraczka (1997), and Pieczka et al. (1998), who used structural analyses and chemical composition as the basis for their models. They concluded that Fe^{2+} occupies *only* the *Y* site in the structure, and argued that previous assignment of Fe^{2+} to the *Z* site simply does not make crystallochemical sense. They assigned the multiple doublets, previously attributed to Fe^{2+} in *Y* and *Z*, to combinations of nearest- and next-nearest neighbors exclusively around the *Y* site. They further proposed that the gradual decrease in quadrupole splitting in successive subcomponents of the $^{Y}Fe^{2+}$ distribution (which is also accompanied by line broadening) is due to the decreasing contributions of ionic bonding in the YO_6 octahedron when cations with higher charge are present as next-nearest neighbors. Subsequent single-crystal XRD analysis of a subset of nine samples studied by Dyar et al. (1998) and Bloodaxe et al. (1999) confirmed that this model was consistent for those samples. They found no evidence for Fe^{2+} occupancy in the *Z* site, consistent with the assignment of Fe^{2+} Mössbauer doublets to the *Y* site in these samples.

FIGURE 7. Unheated and heated (750 °C/30 h) piece of the same Mn-rich crystal (sample MNELB) from Elba Island, Italy. Both polished plates are ~8 mm in length and ~0.6 mm thick.

In the current work, doublets assigned to octahedral Fe^{2+} could, in theory, represent either the three subcomponents of the $^{Y}Fe^{2+}$ distribution or two $^{Y}Fe^{2+}$ distributions and a $^{Z}Fe^{2+}$ distribution, as suggested by Burns (1972) and Saegusa et al. (1979). Distinguishing between these two models in this case requires the X-ray diffraction results. Likewise, the interpretation of Fe spectra that reflect electron delocalization requires that the Fe atoms that are sharing electrons be in adjacent sites. Ferrow (1994) assigned the ED doublets in tourmaline to have isomer shift values of 0.86, 0.84, and 0.71 mm/s for *Y-Y*, *Y-Z*, and *Z-Z* electrons, respectively. The doublet in the present study, which has an area equivalent to 14% and IS = 0.93 mm/s, is (within the error) most consistent with *Y-Y* or possibly *Y-Z* delocalization, because *Z-Z* delocalization would yield a much lower IS and is also less probable in the tourmaline structure (as determined below). If the delocalization occurs between both *Y-Y* and *Y-Z*, in approximately equal proportions, the following configurations should be considered:

Y-Y = $^{Y}Fe^{3+} - {}^{Y}Fe^{2+} \leftrightarrow {}^{Y}Fe^{2+} - {}^{Y}Fe^{3+}$ ($^{Y}Fe^{2+}$ at any time is ~7% of Fe_{tot}).

Y-Z = $^{Y}Fe^{2+} - {}^{Z}Fe^{3+} \leftrightarrow {}^{Y}Fe^{3+} - {}^{Z}Fe^{2+}$ ($^{Z}Fe^{2+}$ at any time is in the range ~0–7% of Fe_{tot}).

Accepting the latter interpretation, the area of the ED doublet would give support for the existence of a small amount (ca. 0–0.23 apfu at any time) of Fe^{2+} at the *Z* site that is in transition due to ED.

An additional interpretation of the Mössbauer spectroscopy is based on the work of Ferrow (1994), which indicates that electrons are more likely to be shared between $^{Y}Fe^{2+}$ and $^{Z}Fe^{3+}$, present at one of the two adjacent *Z* sites as opposed to $^{Z}Fe^{2+} - {}^{Z}Fe^{3+}$ within the spiral chains of the *Z*-centered octahedra. In our Fe^{2+}-rich tourmaline sample (BLS), the electrons are most probably shared between $^{Y}Fe^{2+}$ and $^{Z}Fe^{3+}$, present at one of the two adjacent *Z* sites, equal to $2.02/3 \times 0.78/6 \times 2 \approx 0.18$, whereas for $^{Z}Fe^{2+} - {}^{Z}Fe^{3+}$ delocalization only $0.78/6 \times 0.23/6 \times 2 << 0.01$. These values indicate that ED $^{Y}Fe^{2+} - {}^{Z}Fe^{3+}$ seems to be more probable than $^{Z}Fe^{2+} - {}^{Z}Fe^{3+}$ and, in addition, the latter must be only connected with the less-likely $^{Z}Fe^{2+} - {}^{Z}Fe^{3+}$ clusters within the spiral chains of the *Z*-centered octahedra. Fe^{2+} and Fe^{3+} as well as the remaining octahedrally coordinated ions should be distributed on the *Y* and *Z* sites "statistically," so ascribing the possibility of ED only to the Fe^{2+} and Fe^{3+} pair is not very likely; other ED-cationic-pairs are also probable, e.g., $Fe^{2+} - Ti^{4+}$ or $Mn^{2+} - Fe^{3+}$.

Crystal chemistry and structure analysis

Fe^{2+}-rich tourmaline. Recently, some authors assigned up to ~0.26 apfu Fe^{2+} to the *Z* site in tourmaline of the schorl-dravite series by a minimization procedure that simultaneously accounts for both structural and chemical data (samples 60e, l3l, L3h, Utö; Bosi and Lucchesi 2004; Bosi et al. 2005a, 2005b; Bosi 2008). A Mössbauer interpretation (Andreozzi et al. 2008), which supports these results, is considered questionable (for details see Appendix). The total Fe content of these samples is in the range

~0.8–1.7 apfu, which is distinctly lower than the Fe content of the sample we investigated (~3.3 apfu Fe). Furthermore, there are some issues that make their conclusions more uncertain. In the Mössbauer spectrum of Utö tourmaline, for example, the peak width (Γ) for the doublet with the $^{Z}Fe^{2+}$ assignment is 0.53 mm/s (Bosi 2008), much greater than widths of other peaks that are closer to typical Γ values for silicates of ~0.26–0.30 mm/s. This anomalously large width suggests that the doublet may actually be two or more separate doublets with more typical line widths. The net effect of this would be to decrease the area assigned to $^{Z}Fe^{2+}$ and potentially significantly change the areas in the fit. Bosi (2008) used the quadrupole splitting (QS) of Fe^{3+} = 0.76 mm/s to indicate explicitly that this Fe^{3+} occupies the *Y* site. The doublets of $^{Y}Fe^{3+}$ in tourmalines thermally oxidized in air show QS values changing from about 0.3 mm/s to about 0.9 mm/s, probably corresponding to $^{Y}Fe^{3+}O_4(OH)_2$ converting to $^{Y}Fe^{3+}O_6$, and $^{Z}Fe^{3+}$ from 0.7–0.8 to 1.1–1.3 mm/s corresponding to $^{Z}Fe^{3+}O_5(OH)$ grading to $^{Z}Fe^{3+}O_6$. Thus the doublet of $Fe^{2.5+}$ should be assigned to both the *Y* and *Z* sites. Such an assignment would assume that $^{Z}Fe^{3+}$ cannot cluster with $^{Z}Fe^{2+}$ in the adjacent *Z* sites, because $^{Z}Fe^{2+}$ and $^{Z}Fe^{3+}$ should also be located between two *Z* sites occupied by Al, distinctly predominate at the site over Fe^{3+} or Fe^{2+}.

Bosi (2008) reassigned the site occupancies of tourmalines (sample drv18 and GRAS1) described originally by Cámara et al. (2002) and Ertl et al. (2006b), respectively. Cámara et al. (2002) gave the structural formula of their sample drv18 as $^{X}(Na_{0.49}Ca_{0.48}K_{0.01}\square_{0.02})$ $^{Y}(Mg_{1.35}Fe^{2+}_{0.94}Fe^{3+}_{0.49}Ti^{4+}_{0.20}\square_{0.02})$ $^{Z}(Al_{4.58}Mg_{0.80}Fe^{3+}_{0.62})$ $^{T}(Si_{5.99}Al_{0.01}O_{18})$ $(BO_3)_3$ $^{V}(OH)_3$ $^{W}[F_{0.18}(OH)_{0.18}O_{0.64}]$ and Ertl et al. (2006b) gave the formula of sample GRAS1 as $^{X}(Na_{0.78}K_{0.01}\square_{0.21})$ $^{Y}(Fe^{2+}_{1.89}Al_{0.58}Fe^{3+}_{0.13}Mn^{2+}_{0.13}Ti^{4+}_{0.02}Mg_{0.02}Zn_{0.02}\square_{0.21})$ $^{Z}(Al_{5.74}Fe^{3+}_{0.26})$ $^{T}(Si_{5.90}Al_{0.10}O_{18})$ $(BO_3)_3$ $^{V}(OH)_3$ $^{W}[F_{0.76}(OH)_{0.24}]$. Bosi (2008) gave optimized formulas in which essentially *all* Fe at the *Z* site, originally described as Fe^{3+} in these two samples, is assumed to be Fe^{2+}. For the drv18 and GRAS1 samples, Bosi (2008) calculated *Z*-site occupancies of $^{Z}(Al_{4.58}Mg_{0.81}Fe^{2+}_{0.56}Fe^{3+}_{0.05})$ (drv18) and $^{Z}(Al_{5.60}Fe^{2+}_{0.37}Mg_{0.03})$ (GRAS1), respectively. A simple calculation of theoretical <*Z*-O> bond lengths shows that such occupancies with only $^{Z}Fe^{2+}$ in sample GRAS1, as modeled by Bosi (2008), seems unrealistic. For GRAS1, in which <*Z*-O> is determined to be 1.921 Å (Ertl et al. 2006b), an extrapolative calculation of the theoretical <*Z*-O> bond length, which uses accepted average $^{[6]}Al^{3+}$-O, $^{[6]}Fe^{3+}$-O, and $^{[6]}Fe^{2+}$-O bond lengths in inorganic minerals and compounds (Baur 1981) and a (slightly simplified) refined occupancy of $^{Z}(Al_{5.6}Fe_{0.4})$, gives a theoretical value of <*Z*-O> = 1.916 Å for a completely Fe^{2+}-free *Z* site [i.e., $^{Z}(Al_{5.6}Fe^{3+}_{0.4})$], but 1.924 Å for a Fe^{3+}-free *Z* site [i.e., $^{Z}(Al_{5.6}Fe^{2+}_{0.4})$]. It should be pointed out that for the calculations in the optimization model of Bosi (2008), his own "optimized" octahedral ionic radii for the tourmaline structure were used (Bosi and Lucchesi 2007). For instance, for the radius of Fe^{3+} in tourmaline, Bosi et al. (2005b) and Bosi and Lucchesi (2007) gave values [$r_{Fe^{3+}(Y)}$ = 0.697 Å, $r_{Fe^{3+}(Z)}$ = in the range 0.705 to 0.698 Å], which are, however, considerably larger than the Shannon (1976) value of $r_{Fe^{3+}(HS)}$ = 0.645 Å. Also, the "tourmaline-optimized" values for the Fe^{3+}-O bond lengths given previously, $^{Y}Fe^{3+}$-O = 2.057 Å and $^{Z}Fe^{3+}$-O = 2.055 Å (Bosi and Lucchesi 2004; Bosi et al. 2004), are much higher than the well-established average $^{[6]}Fe^{3+}$-O bond length of 2.011 Å (Baur 1981). Interestingly, the optimized radius values for Fe^{2+}, $r_{Fe^{2+}(Y)}$ = 0.778 Å and $r_{Fe^{2+}(Z)}$ = 0.774 Å (Bosi and Lucchesi 2007), are in good agreement with the Shannon (1976) value of $r_{Fe^{2+}(HS)}$ = 0.78 Å. These obvious contradictions are not addressed by either Bosi (2008) or Bosi and Lucchesi (2007).

Kahlenberg and Veličkov (2000) refined the structure (R = 2.3%) and established the site occupancies of a synthetic, almost Fe^{3+}-free foitite [$Fe^{2+}_{1.53(2)}$ and $Fe^{3+}_{0.05(2)}$ by EMPA and Mössbauer spectroscopy]. This study revealed that the *Z* site is filled exclusively with Al within one standard deviation. They conclude that this result is in accord with an observed <*Z*-O> distance of 1.915 Å, if the determinative relation between the ionic radius of the cation at the *Z* site and <*Z*-O> given by Grice and Ercit (1993) is employed. Kahlenberg and Veličkov (2000) give a bond-valence sum of 2.961 v.u. for the *Z* site, which is very close to the formal valence of 3 v.u. for trivalent Al.

Mn^{2+}-rich tourmaline. A refinement in Bosi et al. (2005a) suggests that the *Z* site with a total of six atom positions contains 0.08 ± 0.02 apfu Mn in their most Mn^{2+}-rich tourmaline sample from Elba Island, Italy (Tsl2g; 9.6 wt% MnO). As stated above, we found no clear evidence for Mn at the *Z* site in a similar tourmaline from Elba Island. However, before assigning the relatively large Mn^{2+} to the *Z* site it seems to be more realistic that the significantly smaller Ti^{4+} will occupy this site. $^{[6]}Ti^{4+}$ has an effective ionic radius that is ~25% smaller than $^{[6]}Mn^{2+}$ (Shannon 1976). Calculation of bond-valence sums for Ti^{4+} in the octahedral sites of the unheated Mn-rich tourmaline demonstrates that Ti^{4+} is slightly closer to its formal valence in the *Z* site (4.65 v.u.) than in the *Y* site (3.33 v.u.). In the heat-treated crystal Ti^{4+} clearly favors the *Y* site, with a bond-valence sum of 3.83 v.u., vs. a sum of 4.58 v.u. in the *Z* site. Moreover, the Mn^{2+} is greatly overbonded at the *Z* site, with bond-valence sums that range between 4.01 and 4.36 v.u. for Mn^{2+} at the *Z* site in these samples. Using the chemical data and the structure refinement, we offer the final structural formula (for the unheated sample) as $^{X}(Na_{0.63}Ca_{0.01}\square_{0.36})$ $^{Y}(Mn^{2+}_{1.30}Al_{1.23}Li_{0.46}Fe^{2+}_{0.01})$ $^{Z}(Al_{5.97}Ti^{4+}_{0.03})$ $^{T}Si_6O_{18}$ $(BO_3)_3$ $^{V}(OH)_3$ $^{W}[F_{0.51}O_{0.45}(OH)_{0.04}]$, with no Mn^{2+} at the *Z* site.

Theoretically, it is also possible that there is a very small amount of Mn^{3+} present in this sample, which could also occupy the *Z* site because of its relatively small effective ionic radius. However, the optical spectra (Fig. 4) indicate that there is very little Mn^{3+} in the yellow regions of the unheated sample, making it unlikely that a significant amount (>1% of the total Mn) of Mn^{3+} will contribute to the structural formula.

In the Austrian Mn^{2+}-rich tourmaline (sample BT in Ertl et al. 2003) there is also no clear evidence that significant amounts of Mn^{2+} or Mn^{3+} occupy the *Z* site. An assessment of inaccuracies in the determination of site occupancy can be examined to establish their magnitude. Because the simultaneous refinement of too large a portion of the total scattering can lead to significant correlations between site occupancy and scale factor, subsequent to the successful refinement detailed above in our new refinements of the Mn-rich tourmalines from Ertl et al. (2003) we fixed the *T* and *B* sites at full occupancy. Releasing the multiplicity of all cation sites (*X*, *Y*, *Z*, *T*, *B*) at the same time, as was done by Bosi et al. (2005a) in the refinements of the Mn-rich tourmalines from Elba, Italy, could be problematic because of the coincident

uncertainties mentioned above. Thus, we consider it likely that this resulted in larger errors in their structural refinements. We conclude that there is no compelling evidence for Mn^{2+} at the *Z* site in tourmaline, even in samples with a relatively high Mn-content (~9 wt% MnO). In addition, the argument of <*Z*-O> distances up to ~1.911 Å as evidence for $^{Z}Mn^{2+}$ (Bosi et al. 2005a) is not convincing because tourmalines with significantly lower Mn^{2+} contents show similar <*Z*-O> distances without any proven occupancy of the *Z* site by Mn. Burns et al. (1994) determined a <*Z*-O> distance of 1.910 Å for a tourmaline with ~6 wt% MnO (no Mg and only 0.02 apfu Fe; sample NP1). Nuber and Schmetzer (1981) described a liddicoatite (with no significant amounts of Fe, Mn, and Mg) with a <Z-O> distance of 1.909 Å. "Oxy-rossmanite" from Austria, the most (natural) Al-rich tourmaline known to date, with only ~2 wt% MnO (and 0.04 apfu Fe^{2+}, no Mg; Ertl et al. 2005), also shows <*Z*-O> distances up to 1.910 Å. Also, Mn^{2+}-rich tourmalines studied by Ertl et al. (2003), which showed no indication of Mn^{2+} on the *Z* site, have slightly enlarged <*Z*-O> distances, up to 1.910 Å. Burns et al. (1994) noted that the scatter in the <*Z*-O> values in the Mn^{2+}-bearing elbaites is presumably due to inductive effects rather than compositional variants. This is in agreement with the curve for the *Z* site produced by Hawthorne et al. (1993).

Data of 54 Al- and Li-bearing tourmaline crystals with refined structures were selected from the literature (Tables 6 and 7, on deposit). In this set of data the <*Z*-O> mean bond length varies from 1.902 to 1.913 Å. For the set of the Li- and Al-bearing tourmalines most of the authors accept that the *Z* site is occupied only by Al (Donnay and Barton 1972; Donnay 1977; Nuber and Schmetzer 1981, 1984; Gorskaya et al. 1982; Grice and Ercit 1993; Burns et al. 1994; MacDonald and Hawthorne 1995; Ertl et al. 1997, 2003, 2004a, 2004b, 2005, 2006a; Selway et al. 1998; Hughes et al. 2000, 2004; Schreyer et al. 2002; Cámara et al. 2002; Marler et al. 2002; Prowatke et al. 2003). However, Bosi et al. (2005a, 2005b), who refined the structure of Mn^{2+}-bearing to Mn^{2+}-rich elbaite and of tourmalines of the elbaite-schorl series, assumed that an increase of the <*Z*-O> distance up to ~1.911 Å is a result of Mn^{2+}-Al or Fe^{2+}-Al disorder. Bosi et al. (2005a) show that Mn-bearing tourmalines from the Elba Island appear to have a good correlation between $^{Y}Mn^{2+}$ and $^{Z}Mn^{2+}$ inferred from their SREF (structure refinement) data. However, a correlation with a similar quality can be obtained for the observed $<^{Z}\text{Al-O}>_{SREF}$ and the total Mn^{2+} content in their Mn^{2+}-rich tourmaline samples (Fig. 8). This correlation indicates a value of about 1.902 Å for Mn^{2+}-free tourmaline, as typical value for <*Z*-O> for crystals with similar ratios among Al, Li, and Mn^{2+}. Thus, the observed difference between this value and the <*Z*-O> distance of their elbaite sample (sample Elb2rim; Bosi et al. 2005a) could be treated as an inductive effect of different *Y*-site and maybe also *T*-site populations (see Ertl et al. 2010b). The *Y*-site population of the elbaite rim (Elb2rim) is quite different from that in the remaining parts of a crystal investigated, in which high amounts of Mn^{2+} are inversely correlated with lithium. Moreover, it is questionable if such a Mn-Al disorder, as it was shown by Bosi et al. (2005a) in their Figures 2 and 3, should be a linear function of the composition. In contrast to this study, we consider the small differences in the <*Z*-O> distances to be due to inductive effects resulting from different *Y*-site populations, i.e., differences in ionic radii of *Y* cations bonded to the O3 and O6 oxygen atoms. In addition, these differences are also related to *T*-site populations, i.e., differences in ionic radii of *T* cations bonded to the O6 and O7 oxygen atoms.

The remarks cited above from the results of Bosi et al. (2005a) and a plot of <*Z*-O> vs. <*Y*-O> co-variation for some Li- and Al-bearing tourmalines (Fig. 10 in Ertl et al. 2010a) indicate a relation between these parameters. Thus, this relation suggests that the population of the *Y*-cations, which have an ionic radius in the range of 0.535 Å ($^{[6]}Al^{3+}$) to 0.83 Å ($^{[6]}Mn^{2+}$), can affect the $<^{Z}\text{Al-O}>$ as observed in the SREF. To elucidate the inductive effects of the different *Y*-site cations as well as the *Y*-site vacancies on the $<^{Z}\text{Al-O}>$ distances, a multiple regression of $<^{Z}\text{Al-O}>_{SREF}$ vs. the amounts of the typical *Y* -site occupants [$N_{Fe^{2+}(Y)}$, $N_{Mn^{2+}(Y)}$, $N_{Mg(Y)}$, $N_{Zn(Y)}$, $N_{Fe^{3+}(Y)}$, $N_{Al(Y)}$, $N_{Li(Y)}$, and $N_{Ti^{4+}(Y)}$] has been tested according to the following equation:

$$<^{Z}\text{Al-O}>_{SREF} = <^{Z}\text{Al-O}>_{Y=vac} + \Sigma N_i C_i$$

where $C_i = <^{Z}\text{Al-O}>_{Y=vac} - <^{Z}\text{Al-O}>_{Y=i}$ and where *i* denotes the different *Y*-site occupants as mentioned above. C_i denotes a change of $<^{Z}\text{Al-O}>$ as induced by the i^{th} *Y*-site cation, measured vs. <*Z*-O> of the ZO_6 octahedron, which is shared with a vacant *Y* site.

For the initial set of data, a good statistical fit of parameters has been achieved ($R > 0.69$; SE < 0.002 Å, MAE ≈ 0.001 Å, Fig. 9a). Except for a few crystals, the values scatter regularly around the line $<^{Z}\text{Al-O}>_{SREF} = <^{Z}\text{Al-O}>_{pred}$. Considering similar values of the estimated parameters C_i for the divalent cations (Fe, Mn, Mg, and Zn), the amounts of these cations have been summarized, and in the final solution the regression of $<^{Z}\text{Al-O}>_{SREF}$ vs. [$N_{Fe^{2+}(Y)+Mn^{2+}(Y)+Mg(Y)+Zn(Y)}$, $N_{Fe^{3+}(Y)}$, $N_{Al(Y)}$, $N_{Li(Y)}$, and $N_{Ti(Y)}$] was

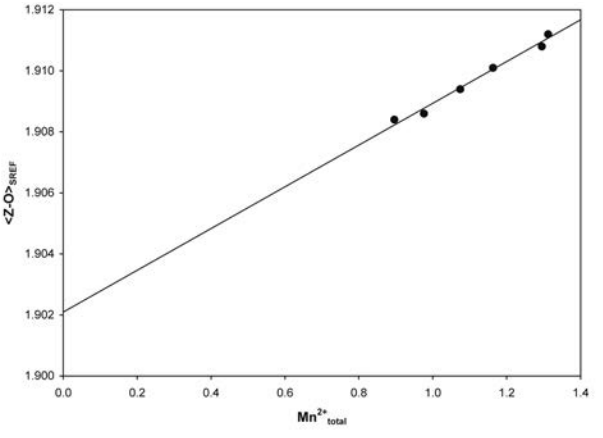

FIGURE 8. Correlation between Mn^{2+} and <*Z*-O> in Mn-rich tourmaline using data from Bosi et al. (2005a).

[1] Deposit item AM-12-057, Tables 6 and 7; CIFs. Deposit items are available two ways: For a paper copy contact the Business Office of the Mineralogical Society of America (see inside front cover of recent issue) for price information. For an electronic copy visit the MSA web site at http://www.minsocam.org, go to the *American Mineralogist* Contents, find the table of contents for the specific volume/issue wanted, and then click on the deposit link there.

examined. After removing outliers (>2 s.d. values; 7 for the first solution, 9 for the second solution for 54 samples; Table 7[1], on deposit), two almost equivalent solutions have been achieved: (1) $<^{Z}\text{Al-O}>_{SREF}$ = 1.8884(71) + 0.0089(24)$N_{Fe^{2+}(Y)+Mn^{2+}(Y)+Mg(Y)+Zn(Y)}$ + 0.0097(391) $N_{Fe^{3+}(Y)}$ +0.0067(25) $N_{Al(Y)}$ + 0.0039(23) $N_{Li(Y)}$ + 0.0136(136) $N_{Ti(Y)}$ with $R \approx 0.83$, $SE = 0.0013$ Å, $MAE = 0.0010$ Å for $n = 47$ crystals, and (2) $<^{Z}\text{Al-O}>_{SREF}$ = 1.8865(67) + 0.0097(23) $N_{Fe^{2+}(Y)+Mn^{2+}(Y)+Mg(Y)+Zn(Y)}$ + 0.0107(367) $N_{Fe^{3+}(Y)}$ + 0.0073(24) $N_{Al(Y)}$ + 0.0045(22) $N_{Li(Y)}$ + 0.0088(128) $N_{Ti(Y)}$, with $R \approx 0.85$, $SE = 0.0013$ Å, $MAE = 0.0010$ Å for $n = 45$ crystals.

Figure 9b presents the $<Z\text{-O}>_{pred}$ vs. $<Z\text{-O}>_{obs}$ co-variation of the second solution. In both solutions, C_0 (1.8884 and 1.8865 Å, respectively) corresponds to a hypothetical <Al-O> distance in the ZO_6 octahedron shared with a vacant *Y* site. The occupation of an i^{th}-cation at the three YO_6 octahedra increases the $<^{Z}\text{Al-O}>$ distance for about C_iN_i, e.g., for elbaite with $Al_{1.5}Li_{1.5}$ the predicted $<^{Z}\text{Al-O}>$ bond length should be ~1.904 Å, for liddicoatite ($AlLi_2$) ~1.903 Å, for dravite and schorl ~1.915–1.916 Å, and for olenite (Al_3) ~1.908 Å. For buergerite this parameter is in the range 1.918–1.919 Å. However, this buergerite value has significant uncertainty because Fe^{3+} is only present in two samples and only in very small amounts (0.02–0.03 apfu). These results also indicate that in (Al,Li)-tourmaline with a deficiency of *Y*-site cations the observed Al-O distance may be slightly lower than 1.904 Å. The results clearly show that Fe^{2+}-Al, Mn^{2+}-Al, or even Mg-Al disorder in (Al,Li)-bearing tourmalines are potentially overestimated because the inductive effect of large *Y*-site cations on the mean size of the smaller ZO_6 octahedron (cations from both sites form bonds with the same O3 and O6 oxygen atoms) is usually not considered. Using this relationship, we can predict the $<Z\text{-O}>$ bond lengths (except for buergerite) within an error of 0.002 Å, or < 1 e.s.d.

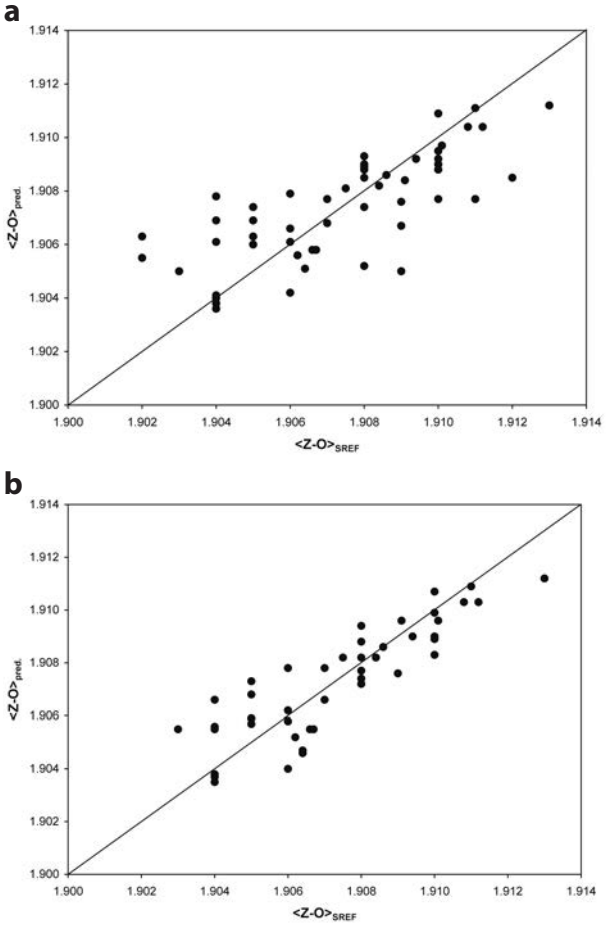

FIGURE 9. (**a**) Initial solution of the correlation between the calculated and the measured <*Z*-O> distances. (**b**) Final solution of the correlation between the calculated and the measured <*Z*-O> distances.

Oxidation experiments

Clark et al. (2008) stated that although the <B-O> bond length is reasonably constant for all tourmaline species, the B-O2 and B-O8 bond lengths are not, but vary according to the chemical composition of the tourmaline. The observed B-O2/B-O8 ratios compared between the natural (~0.99) and the oxidized (~1.01) Fe^{3+}-rich tourmaline (Table 3) are very similar to the values described by Clark et al. (2008) for schorl and buergerite, respectively. The structural data of this "synthetic" buergerite is very similar to data of natural buergerite except that there is three times as much Fe^{3+} at the *Z* site (for comparison with structural data of buergerite from Mexico see Barton 1969; Grice and Ercit 1993; updated chemical data in Dyar et al. 1998). Oxidation experiments (at 700 °C) on Fe^{2+}-rich tourmalines by Bačik et al. (2011a) resulted in tourmalines similar to buergerite. These authors described the substitution vector for oxidation of Fe as $Fe^{3+}OFe^{2+}_{-1}(OH)_{-1}$.

We conclude that there is no convincing proof that Fe^{2+} occupies the *Z* site, apart from that occupancy connected with delocalization of hopping electrons involving Fe cations at the *Y* and *Z* sites. We further conclude that there is no convincing proof for Mn^{2+} at the *Z* site. We consider that an unequivocal explanation of the reasons for the elongation of $<Z\text{-O}>$ is also necessary for a correct assumption of the cation populations at the *Y* and *Z* sites, and for the evaluation of any possible disorder in the tourmaline structure. Inductive effects in the structure seem to have a significant influence to the $<Z\text{-O}>$ bond length.

ACKNOWLEDGMENTS

We thank G. Knobloch, Aggsbach-Dorf, Austria, for providing the Fe-rich tourmaline sample and A. Wagner, Vienna, Austria, for preparing the samples. The authors thank E.S. Grew, G. Redhammer, F. Bosi, and R. Thompson for helpful comments on an early version of this manuscript. We sincerely thank S.J. Mills, G. Harlow, and an anonymous reviewer for their constructive comments on the manuscript. This work was supported in part by Austrian Science Fund (FWF) projects no. P20509-N10 and no. P23012-N19, by NASA grant NNG04GG12G to M.D.D. and National Science Foundation (U.S.A) grants EAR-0003201, EAR-9804768, and NSF-MRI 1039436 to J.M.H. and EAR-0337816 to G.R.R.

REFERENCES CITED

Andreozzi, G.B., Bosi, F., and Longo, M. (2008) Linking Mössbauer and structural parameters in elbaite-schorl-dravite tourmalines. American Mineralogist, 93, 658–666.

Aurisicchio, C. and Pezzotta F. (1997) Tourmaline-group minerals of the LCT miarolitic pegmatites of the Elba island (Italy): chemical composition and genetic and paragenetic inferences. Abstract volume of the congress "Tourmaline '97", Moravian Museum Brno, Czech Republic, University of Manitoba, Winnipeg, Canada, 1–2.

Bačik, P., Ozdín, D., Miglierini, M., Kardošová, P., Pentrák, M., and Haloda, J. (2011a) Crystallochemical effects of heat treatment on Fe-dominant tourmalines from Dolní Bory (Czech Republic) and Vlachovo (Slovakia). Physics and Chemistry of Minerals, 38, 599–611.

Bačik, P., Cempírek, J., Uher, P., Ozdín, D., Filip, J., Novák, M., Škoda, R., Breiter,

K., Klementová, M., and Ďud'a, R. (2011b) Oxy-schorl, IMA 2011-011. CNMNC Newsletter no. 10, October, 2011, p. 2550. Mineralogical Magazine, 75, 2549–2561.
Barton, R. Jr. (1969) Refinement of the crystal structure of buergerite and the absolute orientation of tourmalines. Acta Crystallographica, B25, 1524–1533.
Baur, W.H. (1981) Interatomic distance predictions for computer simulation of crystal structures. In M. O'Keeffe and A. Navrotsky, Eds., Structure and Bonding in Crystals, vol. II, chapter 15, p. 31–52. Academic Press, New York.
Bloodaxe, E.S., Hughes, J.M., Dyar, M.D., Grew, E.S., and Guidotti, C.V. (1999) Linking structure and chemistry in the schorl-dravite series. American Mineralogist, 84, 922–928.
Bosi, F. (2008) Disordering of Fe^{2+} over octahedrally coordinated sites of tourmaline. American Mineralogist, 93, 1647–1653.
Bosi, F. and Lucchesi, S. (2004) Crystal chemistry of the schorl-dravite series. European Journal of Mineralogy, 16, 335–344.
——— (2007) Crystal chemical relationships in the tourmaline group: Structural constraints on chemical variability. American Mineralogist, 92, 1050–1063.
Bosi, F., Lucchesi, S., and Reznitskii, L. (2004) Crystal chemistry of the dravite-chromdravite series. European Journal of Mineralogy, 16, 345–352.
Bosi, F., Agrosì, G., Lucchesi, S., Melchiorre, G., and Scandale, E. (2005a) Mn-tourmaline from island of Elba (Italy): Crystal chemistry. American Mineralogist, 90, 1661–1668.
Bosi, F., Andreozzi, G.B., Federico, M., Graziani, G., and Lucchesi, S. (2005b) Crystal chemistry of the elbaite-schorl series. American Mineralogist, 90, 1784–1792.
Bosi, F., Skogby, H., Scandale, E., and Agros, G. (2011) Tsilaisite, IMA 2011-047. CNMNC Newsletter no. 10, October 2011, p. 2559; Mineralogical Magazine, 75, 2549–2561.
Bruker AXS Inc. (2001) SaintPlus, ver. 6.45. Bruker AXS Inc., Madison, Wisconsin.
Burns, P.C., MacDonald, D.J., and Hawthorne, F.C. (1994) The crystal chemistry of manganese-bearing elbaite. Canadian Mineralogist, 32, 31–41.
Burns, R.G. (1972) Mixed valencies and site occupancies of iron in silicate minerals from Mössbauer spectroscopy. Canadian Journal of Spectroscopy, 17, 51–59.
Cámara, F., Ottolini, L., and Hawthorne, F.C. (2002) Chemistry of three tourmalines by SREF, EMPA, and SIMS. American Mineralogist, 87, 1437–1442.
Cempírek, J., Novák, M., Ertl, A., Hughes, J.M., Rossman, G.R., and Dyar, M.D. (2006) Fe-bearing olenite with tetrahedrally coordinated Al from an abyssal pegmatite of the Bohemian massif at Kutná Hora: Structure, crystal chemistry, and optical spectra. Canadian Mineralogist, 44, 23–30.
Clark, C.M., Wadoski, E.R., and Freeman, E.D. (2008) Tourmaline chemistry and the $^{[3]}$B site. American Mineralogist, 93, 409–413.
Donnay, G. (1977) Structural mechanism of pyroelectricity in tourmaline. Acta Crystallographica, A33, 927–932.
Donnay, G. and Barton, R. Jr. (1972) Refinement of the crystal structure of elbaite and the mechanism of tourmaline solid solution. Tschermaks Mineralogische und Petrographische Mitteilungen, 18, 273–286.
Dyar, M.D., Taylor, M.E., Lutz, T.M., Francis, C.A., Guidotti, C.V., and Wise, M. (1998) Inclusive chemical characterization of tourmaline: Mössbauer study of Fe valence and site occupancy. American Mineralogist, 83, 848–864.
Dyar, M.D., Wiedenbeck, M., Robertson, D., Cross, L.R., Delaney, J.S., Ferguson, K., Francis, C.A., Grew, E.S., Guidotti, C.V., Hervig, R.L., and others. (2001) Reference minerals for the microanalysis of light elements. Geostandards Newsletter, 25, 441–463.
Ertl, A. (1995) Elbait, Olenit, Dravit-Buergerit-Mischkristalle, Dravit, Uvit und ein neuer Al-Turmalin (?) von österreichischen Fundstellen. Mitteilungen der Österreichischen Mineralogischen Gesellschaft, 140, 55–72.
Ertl, A., Pertlik, F., and Bernhardt, H.-J. (1997) Investigations on olenite with excess boron from the Koralpe, Styria, Austria. Österreichische Akademie der Wissenschaften, Mathematisch-Naturwissenschaftliche Klasse, Abteilung I, Anzeiger, 134, 3–10.
Ertl, A., Hughes, J.M., Prowatke, S., Rossman, G.R., London, D., and Fritz, E.A. (2003) Mn-rich tourmaline from Austria: structure, chemistry, optical spectra, and relations to synthetic solid solutions. American Mineralogist, 88, 1369–1376.
Ertl, A., Pertlik, F., Dyar, M.D., Prowatke, S., Hughes, J.M., Ludwig, T., and Bernhardt, H.-J. (2004a) Olenite with tetrahedrally coordinated Fe^{3+} from Eibenstein, Austria: structural, chemical, and Mössbauer data. Canadian Mineralogist, 42, 1057–1063.
Ertl, A., Schuster, R., Prowatke, S., Brandstätter, F., Ludwig, T., Bernhardt, H.-J., Koller, F., and Hughes, J.M. (2004b) Mn-rich tourmaline and fluorapatite in a Variscan pegmatite from Eibenstein an der Thaya, Bohemian massif, Lower Austria. European Journal of Mineralogy, 16, 551–560.
Ertl, A., Rossman, G.R., Hughes, J.M., Prowatke, S., and Ludwig, T. (2005) Mn-bearing "oxy-rossmanite" with tetrahedrally-coordinated Al and B from Austria: structure, chemistry, and infrared and optical spectroscopic study. American Mineralogist, 90, 481–487.
Ertl, A., Hughes, J.M., Prowatke, S., Ludwig, T., Prasad, P.S.R., Brandstätter, F., Körner, W., Schuster, R., Pertlik, F., and Marschall, H. (2006a) Tetrahedrally-coordinated boron in tourmalines from the liddicoatite-elbaite series from Madagascar: Structure, chemistry, and infrared spectroscopic studies. American Mineralogist, 91, 1847–1856.
Ertl, A., Kolitsch, U., Prowatke, S., Dyar, M.D., and Henry, D.J. (2006b) The F-analogue of schorl from Grasstein, Trentino—South Tyrol, Italy: Crystal structure and chemistry. European Journal of Mineralogy, 18, 583–588.
Ertl, A., Kolitsch, U., Meyer, H.-P., Ludwig, T., Lengauer, C.L., Nasdala, L., and Tillmanns, E. (2009) Substitution mechanism in tourmalines of the "fluor-elbaite"-rossmanite series from Wolkenburg, Saxony, Germany. Neues Jahrbuch für Mineralogie Abhandlungen, 186, 51–61.
Ertl, A., Rossman, G.R., Hughes, J.M., London, D., Wang, Y., O'Leary, J.A., Dyar, M.D., Prowatke, S., Ludwig, T., and Tillmanns, E. (2010a) Tourmaline of the elbaite-schorl series from the Himalaya Mine, Mesa Grande, California, U.S.A.: A detailed investigation. American Mineralogist, 95, 24–40.
Ertl, A., Hughes, J.M., and Tillmanns, E. (2010b) The correct formula for Mg- and Fe^{3+}-tourmaline: the influence of the <*T*-O> distance on the <*Z*-O> bond length. Acta Mineralogica-Petrographica Abstract Series, Volume 6, 476, IMA2010 20th General Meeting of the International Mineralogical Association, 21–27 August 2010, Budapest, Hungary.
Ferrow, E.A. (1994) Mössbauer effect study of the crystal chemistry of tourmaline. Hyperfine Interactions, 91, 689–695.
Ferrow, E.A., Annersten, H., and Gunawardane, R.P. (1988) Mössbauer effect study on the mixed valence state of iron in tourmaline. Mineralogical Magazine, 52, 221–228.
Fischer, R.X. and Tillmanns, E. (1988) The equivalent isotropic displacement factor. Acta Crystallographica, C44, 775–776.
Fortier, S. and Donnay, G. (1975) Schorl refinement showing composition dependence of the tourmaline structure. Canadian Mineralogist, 13, 173–177.
Francis, C.A., Dyar, M.D., Williams, M.L., and Hughes, J.M. (1999) The occurrence and crystal structure of foitite from a tungsten-bearing vein at Copper Mountain, Taos County, New Mexico. Canadian Mineralogist, 37, 1431–1438.
Fuchs, G. and Matura, A. (1976) Zur Geologie des Kristallins der Böhmischen Masse. Jahrbuch der Geologischen Bundesanstalt, 119, 1–43.
Gorskaya, M.G., Frank-Kamenetskaya, O.V., Rozhdestvenskaya, I.V., and Frank-Kamenetskii, V.A. (1982) Refinement of the crystal structure of Al-rich elbaite, and some aspects of the crystal chemistry of tourmalines. Soviet Physics Crystallography, 27, 63–66.
Grice, J.D. and Ercit, T.S. (1993) Ordering of Fe and Mg in the tourmaline crystal structure: The correct formula. Neues Jahrbuch für Mineralogie Abhandlungen, 165, 245–266.
Hatert, F. and Burke, E.A.J. (2008) The IMA–CNMNC dominant-constituent rule revisited and extended. Canadian Mineralogist, 46, 717–728.
Hawthorne, F.C. (1996) Structural mechanisms for light-element variations in tourmaline. Canadian Mineralogist, 34, 123–132.
——— (2002) Bond-valence constraints on the chemical composition of tourmaline. Canadian Mineralogist, 40, 789–797.
Hawthorne, F.C. and Henry, D.J. (1999) Classification of the minerals of the tourmaline group. European Journal of Mineralogy, 11, 201–215.
Hawthorne, F.C., MacDonald, D.J., and Burns, P.C. (1993) Reassignment of cation site-occupancies in tourmaline: Al-Mg disorder in the crystal structure of dravite. American Mineralogist, 78, 265–270.
Henry, D., Novák, M., Hawthorne, F.C., Ertl, A., Dutrow, B.L., Uher, P., and Pezzotta, F. (2011) Nomenclature of the tourmaline-supergroup minerals. American Mineralogist, 96, 895–913.
Hughes, J.M., Ertl, A., Dyar, M.D., Grew, E., Shearer, C.K., Yates, M.G., and Giudotti, C.V. (2000) Tetrahedrally coordinated boron in a tourmaline: Boron-rich olenite from Stoffhütte, Koralpe, Austria. Canadian Mineralogist, 38, 861–868.
Hughes, J.M., Ertl, A., Dyar, M.D., Grew, E., Wiedenbeck, M., and Brandstätter, F. (2004) Structural and chemical response to varying $^{[4]}$B content in zoned Fe-bearing olenite from Koralpe, Austria. American Mineralogist, 89, 447–454.
Kahlenberg, V. and Veličkov, B. (2000) Structural investigations on a synthetic alkali-free hydrogen-deficient Fe-tourmaline (foitite). European Journal of Mineralogy, 12, 947–953.
Kraczka, J. and Pieczka, A. (2000) Mössbauer study of thermal oxidation of Fe^{2+} in tourmaline. Molecular Physics Reports, 30, 80–85.
MacDonald, D.J. and Hawthorne, F.C. (1995) The crystal chemistry of Si ⇔ Al substitution in tourmaline. Canadian Mineralogist, 33, 849–858.
Marler, B., Borowski, M., Wodara, U., and Schreyer, W. (2002) Synthetic tourmaline (olenite) with excess boron replacing silicon in the tetrahedral site: II. Structure analysis. European Journal of Mineralogy, 14, 763–771.
Mattson, S.M. and Rossman, G.R. (1986) Yellow, Mn-rich elbaite with Mn-Ti intervalence charge transfer. American Mineralogist, 71, 599–602.
——— (1987) Fe^{2+}-Fe^{3+} interactions in tourmaline. Physics and Chemistry of Minerals, 14, 163–171.
——— (1988) Fe^{2+}-Ti^{4+} charge transfer in stoichiometric Fe^{2+}, Ti^{4+}-minerals. Physics and Chemistry of Minerals, 16, 78–82.
Nonius (2007) COLLECT; DENZO-SMN. Nonius BV, Delft, The Netherlands.
Nuber, B. and Schmetzer, K. (1981) Strukturverfeinerung von Liddicoatit. Neues

Jahrbuch für Mineralogie Monatshefte, 215–219.
——— (1984) Structural refinement of tsilaisite (manganese tourmaline). Neues Jahrbuch für Mineralogie Monatshefte, 301–304.
Orlandi, P. and Pezzotta F. (1996) Minerali dell'Isola d'Elba, i minerali dei giacimenti metalliferi dell'Elba orientale e delle pegmatiti del M.te Capanne. Ed. Novecento Grafico, Bergamo, Italy. 248 pp.
Otwinowski, Z., Borek, D., Majewski, W., and Minor, W. (2003) Multiparametric scaling of diffraction intensities. Acta Crystallographica, A59, 228–234.
Pieczka, A. (1997) Statistical interpretation of structural parameters of tourmaline iron ordering in octahedral sites. Tourmaline 1997 International Symposium on Tourmaline, Nové Mesto na Morave, Czech Republic, 70–71.
Pieczka, A. and Kraczka, J. (1997) Thermal oxidation of Fe^{2+} ions in the schorl-dravite series and its significance in the analysis of distribution of Fe^{2+} octahedral ions. Tourmaline 1997 International Symposium on Tourmaline, Nové Mesto na Morave, Czech Republic, 72–73.
——— (2001) X-ray and Mössbauer study of Fe^{2+} thermal oxidation in Fe-Mg-Al-tourmaline. Bulletin Liaison S.F.M.C., 13, 42–43.
——— (2004) Oxidized tourmalines—a combined chemical, XRD and Mössbauer study. European Journal of Mineralogy, 16, 309–321.
Pieczka, A., Kraczka, J., and Żabiński, W. (1998) Mössbauer spectra of Fe^{3+}-poor schorls: reinterpretation on the basis of ordered structure model. Journal of the Czech Geological Society, 43, 69–74.
Pouchou, J.L. and Pichoir, F. (1991) Quantitative analysis of homogenous or stratified microvolumes applying the model "PAP". In K.F.K. Heinrich and D.E. Newbury, Eds., Electron Probe Quantitation, p. 31–75. Plenum Press, New York.
Prowatke, S., Ertl, A., and Hughes, J.M. (2003) Tetrahedrally-coordinated Al in Mn-rich, Li- and Fe-bearing olenite from Eibenstein an der Thaya, Lower Austria: A chemical and structural investigation. Neues Jahrbuch für Mineralogie Monatshefte, 9, 385–395.
Saegusa, N., Price, D.X., and Smith, G. (1979) Analysis of the Mössbauer spectra of several iron-rich tourmalines (schorls). Journal de Physique, 40, C2-456–C2-459.
Schreyer, W., Hughes, J.M., Bernhardt, H.-J., Kalt, A., Prowatke, S., and Ertl, A. (2002) Reexamination of olenite from the type locality: detection of boron in tetrahedral coordination. European Journal of Mineralogy, 14, 935–942.
Selway, J.B., Novák, M., Hawthorne, F.C., Černý, P., Ottolini, L., and Kyser, T.K. (1998) Rossmanite, $\square(LiAl_2)Al_6Si_6O_{18}(BO_3)_3(OH)_4$, a new alkali-deficient tourmaline: description and crystal structure. American Mineralogist, 83, 896–900.
Shannon, R.D. (1976) Revised effective ionic radii and systematic studies of interatomic distances in halides and chalcogenides. Acta Crystallographica, A32, 751–767.
Sheldrick, G.M. (2008) A short history of *SHELX*. Acta Crystallographica, A64, 112–122.
Wivel, C. and Mørup, S. (1981) Improved computational procedure for evaluation of overlapping hyperfine parameter distributions in Mössbauer spectra. Journal of Physics E: Scientific Instrumentation, 14, 605–610.

Manuscript received October 18, 2011
Manuscript accepted May 3, 2012
Manuscript handled by Aaron Celestian

Appendix

Andreozzi et al. (2008) described a doublet (ΔEQ = 1.38 mm/s) that they consider consistent with Fe^{2+} at the *Z* octahedron, which is smaller and less distorted than the *Y* octahedron (λZ = 1.014, λY = 1.024). This interpretation is problematic, and there are several issues with some of their fits.

(1) In four of the spectra, some values of the peak width (Γ) are anomalously small, e.g., below 0.24–0.25 mm/s, the smallest acceptable peak width for a single line in a quadrupole doublet (J. Kraczka, personal communication, 2000). Additionally, successive lines in a spectrum should be broader when the value for quadrupole splitting (QS) decreases, which is commonly the case when there is a decrease in intensity/abundance of a line/quadrupole. Such a line/quadrupole is much less defined than lines with higher QS and usually higher intensity. Hence, such lines with an anomalous Γ value are more frequent in the data.

(2) These authors further do not explain the reason that quadrupoles with almost the same isomer shift (IS) and QS values are interpreted in a different way. For example, the interpretation of the curve fits of samples 61Vbh and 62ha (rim) are different: in the first sample quadrupole with IS = 1.09 mm/s and QS = 2.39 mm/s was assigned to Fe^{2+}(Y1), but in the second sample quadrupole with IS = 1.09 mm/s and QS = 2.35 mm/s is related to Fe^{2+}(Y2). Both samples represent Li-bearing tourmalines, so almost the same values of the parameters suggest similar structural environments of Fe^{2+} both in the Y1 and Y2 positions. This is inconsistent because both positions should have two distinctly different surroundings.

(3) For the samples 62ha (rim) and 64gh (core) a quadrupole with IS between 1.15–1.19 mm/s and QS = 1.83–1.90 mm/s is interpreted as Fe^{2+}(Y3), but the same assignment has a quadrupole with IS = 1.05 mm/s and QS = 1.55 mm/s found in the spectrum of the L2al crystal. Furthermore, in other crystals, a quadrupole with QS varying from 1.45 (a value close to 1.55 mm/s) to 1.29 mm/s is related to Fe^{2+} at the *Z* site. Such variations of the QS values is more likely due to variations of the *W*-site occupation, because this site can be mainly occupied by OH or F, but it also can be occupied just by O (e.g., *oxy*-varieties). In such a situation, the *Y* site occupied by Fe^{2+} can have a similar first-coordination sphere as Fe^{2+} apparently located at the *Z* site (O_5OH).

(4) There is some confusion in explaining the $Fe^{2.5+}$ quadrupole(s). This quadrupole corresponds to electron hopping between two cations with different valence states, e.g., in the pairs Fe^{2+}-Fe^{3+}, Fe^{2+}-Ti^{4+}, Fe^{3+}-Mn^{2+}, etc. and such Fe is defined as 2.5+ v.u. Theoretically, IS and QS of a quadrupole (as mentioned above) with the presence of $Fe^{2.5+}$ should have mean values, respectively, of parameters characteristic of Fe^{2+} and Fe^{3+} in 6-coordination. Thus, a $Fe^{2.5+}$ quadrupole doublet should have a characteristic IS close to 0.70–0.75 mm/s, regardless of the location of Fe^{2+} and Fe^{3+} cations in the tourmaline structure. Typical IS values of Fe^{2+} and of Fe^{3+} vary from 1.09–1.02 mm/s and from 0.30–0.45 mm/s, respectively. However some authors, e.g., Ferrow et al. (1988) and Andreozzi et al. (2008) themselves, accept significantly different IS values for the quadrupole, reaching even 0.96 mm/s. Such values are very close to the lowest IS values accepted for $^{VI}Fe^{2+}$ and might indicate a resolution that should not be accepted as the final result. Such a value might be an indication for the need of subsequent fits with an additional Fe^{2+}-quadrupole with a low QS value, and Fe^{3+}- and $Fe^{2.5+}$-quadrupoles. Andreozzi et al. (2008) present for samples 60e and 65e a doublet assigned to $^{Z}Fe^{2+}$ with a very low IS close to 0.97–0.99 mm/s and a very similar doublet assigned to $Fe^{2.5+}$(Y-Z or Y-Y) with IS close to 0.92–0.96 mm/s. It is questionable that such a difference between the doublets allows such a different assignment.

(5) The $Fe^{2.5+}$-quadrupole can only occur in a spectrum with the simultaneous presence of Fe^{3+}-quadrupole(s). Because, when a spectrum shows only a $Fe^{2.5+}$-quadrupole, the entire Fe^{3+} should be clustered in the surrounding octahedron filled with Fe^{2+}. It shares a common edge with the octahedron that is occupied by Fe^{3+}. However, it is unlikely that the entire Fe^{3+} content would be placed in an adjacent site to the Fe^{2+} octahedron. For example, the three *Y* sites of the *Y*-octahedra triad ("*Y*-*Y*" charge transfer) can be occupied in many variants like $Fe^{2+}Fe^{2+}Fe^{2+}$ or $Fe^{2+}Fe^{2+}Fe^{3+}$ with possible charge transfer between Fe^{2+} and Fe^{3+}, or $Fe^{2+}Fe^{3+}Fe^{3+}$ also with possible charge transfer, but with

an excess of Fe^{3+}, or $Fe^{3+}Fe^{3+}Fe^{3+}$ for which charge transfer is impossible, Fe^{3+} doublets must occur in the spectrum. There are also many other variants of the triad for which the charge transfer process is impossible, e.g., $MgMgFe^{3+}$, $MgFe^{3+}Fe^{3+}$, $AlAlFe^{3+}$, $AlFe^{3+}Fe^{3+}$, etc. Thus, it is not likely that the entire Fe^{3+} present in the triad is clustered with Fe^{2+}. A similar situation is in the case of ${}^{Z}Fe^{2+}-{}^{Z}Fe^{3+}$ charge transfer. Fe^{3+} from such *Z* sites must also occur in short-range structures obviating the presence of Fe^{3+} in the second coordination sphere.

(6) Further, it is not clear if the charge transfer process at the *Z* sites is possible. Assuming the presence of Fe^{2+} at the *Z* site, the transition ${}^{Z}Fe^{2+}-{}^{Z}Fe^{3+}$ (also ${}^{Y}Fe^{2+}-{}^{Y}Fe^{3+}$) is only theoretically possible, because the presence of both cations in two adjacent *Z* sites is almost impossible, i.e., the probability of such structural variant is almost equal to zero.

(7) In many tourmaline samples from Andreozzi et al. (2008) abundances for Fe^{3+} are relatively high. However, charge transfer processes are invisible in these samples (29% Fe^{3+} in L4aa, 47% Fe^{3+} in L3l, 11% Fe^{3+} in 235b, 14% Fe^{3+} in 84a, 31% Fe^{3+} in 112a, 28% Fe^{3+} in 233g), but conversely, the charge transfer quadrupole has been detected in samples for which no Fe^{3+}-quadrupole has been observed (e.g., 9% $Fe^{2.5+}$ in sample L2al). Such an interpretation is questionable.

In conclusion, we consider the Mössbauer fits from Andreozzi et al. (2008) to be imprecise and of limited use in evaluating the possibility of having disorder of Fe^{2+} between the *Y* and the *Z* sites. Moreover, it is important to recognize that site assignments based on Mössbauer spectroscopy do not provide unequivocal evidence unless they are firmly based on other types of data (usually single-crystal structure refinements).